SOD1^{A4V} aggregation alters ubiquitin homeostasis in a cell model of ALS

Natalie E. Farrawell[1,2], Isabella Lambert-Smith[1,2], Kristen Mitchell[1,2], Jessie McKenna[3], Luke McAlary[1,2,4], Prajwal Ciryam[5,6,7], Kara L. Vine[1,2], Darren N. Saunders[3], Justin J. Yerbury[1,2*]

[1]Illawarra Health and Medical Research Institute, Wollongong, NSW, Australia
[2]School of Biological Sciences, Centre of Medicine and Molecular Bioscience, University of Wollongong, Northfields Ave, Wollongong, NSW, Australia, 2522
[3]School of Medical Sciences, Faculty of Medicine, UNSW Australia
[4]Department of Physics & Astronomy, University of British Columbia, Vancouver, British Columbia, Canada.
[5]Department of Chemistry, University of Cambridge, Cambridge CB2 1EW, UK
[6]Department of Molecular Biosciences, Rice Institute for Biomedical Research, Northwestern University, Evanston, IL 60208-3500, USA
[7]Department of Neurology, Columbia University College of Physicians & Surgeons, New York, NY 10032-3784

*** Correspondence:**
Dr Justin John Yerbury
Illawarra Health and Medical Research Institute
Northfields Ave, Wollongong, NSW, 2522, Australia.
Ph: 61-2-42981534; Email: jyerbury@uow.edu.au

Keywords: protein aggregation, ubiquitin, SOD1, ALS, supersaturation, proteostasis, neurodegeneration, ubiquitomics, degron, proteasome.

Abstract

Amyotrophic lateral sclerosis (ALS) is a fatal neurodegenerative disease involving the selective death of upper and lower motor neurons in the primary motor cortex and spinal cord. A hallmark of ALS pathology is the accumulation of ubiquitinated protein inclusions within motor neurons. Previous studies suggest the sequestration of ubiquitin (Ub) into inclusions reduces the availability of free Ub, which is essential for cellular function and survival. However, the dynamics of the Ub landscape in ALS have not yet been described. Here we show that Ub homeostasis is altered in a SOD1 cell model of ALS. Utilising fluorescently tagged Ub, we followed the distribution of Ub in living cells expressing SOD1 and show that Ub is present at the earliest stages of SOD1 aggregation. We also report that cells containing aggregates of mutant SOD1 have greater ubiquitin-proteasome system (UPS) dysfunction as measured by the accumulation of the fluorescent proteasome reporter tdTomato^{CL1}. Furthermore, SOD1 aggregation is associated with the redistribution of Ub and depletion of the free Ub pool. Ubiquitomics analysis indicates that mutant SOD1 is associated with a shift of Ub to a pool of supersaturated proteins including those associated with oxidative phosphorylation and metabolism, corresponding with altered mitochondrial morphology and function. Taken together, these results suggest misfolded SOD1 contributes to UPS dysfunction and that Ub homeostasis is an important target for monitoring pathological changes in ALS.

Background

Amyotrophic lateral sclerosis (ALS, also known as motor neuron disease, MND) is a progressive neurodegenerative disease leading to paralysis of voluntary muscles due to the death of motor neurons in the brain and spinal cord. The prognosis of ALS is poor, usually leading to death within 2 to 5 years of first symptoms. A fraction of patients also develop clinical or subclinical frontotemporal dementia (FTD) [1]. In most cases of ALS, the cause remains unknown (sporadic ALS; sALS). However, approximately 10% of cases are inherited (familial ALS; fALS). A large proportion (20%) of fALS cases can be attributed to mutations in the gene encoding superoxide dismutase 1 (SOD1) [2]. SOD1 was the first gene discovered to cause fALS and is also the most widely studied. There are now over 20 genes known to cause ALS [2] including a growing list of genes associated with dysregulation of ubiquitin (Ub) signalling. Genetic mutations in VCP, SQSTM1, UBQLN2, OPTN have all been associated with ALS, and are all part of the cell's protein degradation machinery. In addition, recently discovered mutations in TBK1 [3] and CCNF [4] add to this growing list of degradation machinery associated with ALS. The precise role of each of these genes in the homeostasis of Ub is unknown, but Ub sequestration into insoluble inclusions is common to all forms of ALS [5].

Abnormal accumulation of proteins into insoluble aggregates is a hallmark of many neurodegenerative diseases, including Alzheimer's disease, Parkinson's disease Huntington's disease and ALS [6]. In the context of ALS, there is growing evidence that a correlation exists between protein aggregate load and neuronal loss in ALS spinal cord [7-11]. Our previous work showed a correlation between *in vitro*

aggregation propensity and rate of disease progression [12], suggesting that protein aggregates are intimately linked with motor neuron cell death. Recent work also indicates that protein misfolding and aggregation may be responsible for disease progression through a prion like propagation throughout the nervous system [11, 13-16]. It is unlikely that misfolding alone is responsible for the disease and that post translational modifications play an important role [17]. One crucial post translational modification is ubiquitination, necessary for protein degradation. Degradation defects that lead to inclusion formation are associated with a tendency for cells to be dysfunctional and undergo apoptosis [18-20].

Inclusions associated with neurodegeneration consist of a variety of proteins including proteins specific to the disease (e.g. Aβ and tau in Alzheimer's disease [21]), proteins associated with cellular quality control machinery (e.g. molecular chaperones [22, 23] and the proteasome [24]) and other unrelated aggregation prone proteins [25, 26]. Based on analysis of human tissue, it has been shown that a large number of proteins are supersaturated in the cell, with cellular concentrations under wild-type conditions that exceed their predicted solubility [25, 26]. These supersaturated proteins are associated with the biochemical pathways underpinning a variety of neurodegenerative diseases. Most recently, we have shown that proteins co-aggregating with SOD1, TDP-43, and FUS inclusions are supersaturated [5], consistent with a collapse of motor neuron protein homeostasis in ALS. Others have found that the proteins that co-aggregate with c9orf72 dipeptide repeats in cell models are also supersaturated [27]. The composition of inclusions found in ALS varies considerably depending on whether the disease is sporadic or familial, and the genetics of the familial forms.

100

101 Ub is a pervasive feature of inclusions in ALS, regardless of underlying genetic
102 aetiology. Ub is a versatile signalling molecule responsible for controlling an array of
103 cellular pathways including transcription, translation, vehicle transport and apoptosis
104 [28]. Ub labels substrate proteins via a highly ordered multi-step enzymatic cascade
105 with specific differences in the length and topology of poly-ubiquitin chains
106 determining a range of signalling outcomes, including proteolytic degradation via the
107 proteasome [29, 30]. Inside cells, Ub exists in a dynamic equilibrium between free Ub
108 and Ub conjugates and is controlled by the opposing actions of Ub ligases and
109 deubiquitinating enzymes (DUBS) [31, 32]. It has been proposed that the
110 sequestration of Ub into insoluble aggregates may deplete the free Ub pool required
111 by many essential cellular processes [32].

112

113 Although mounting genetic and functional evidence suggests an important role for the
114 UPS in the development of ALS pathology, the distribution and availability of Ub in
115 ALS models has not yet been described. In the work reported here, we sought to
116 characterise the Ub landscape in a cell-based SOD1 model of ALS **(Figure 1)**. We
117 show that Ub homeostasis is disrupted in cells containing SOD1 aggregates by
118 following the distribution of fluorescently labelled Ub in live cells expressing SOD1.
119 The aggregation of mutant SOD1 leads to an accumulation of the proteasome reporter
120 tdTomato^{CL1}, indicative of UPS dysfunction. This dysfunction was further supported
121 by the redistribution of the Ub pool and decrease in free Ub levels observed in cells
122 with SOD1 aggregates. Moreover, ubiquitome analysis confirmed misfolded SOD1
123 was associated with Ub redistribution and subsequent alterations to mitochondrial
124 morphology. This report highlights that disruption to Ub homeostasis is associated

125 with aggregation of misfolded proteins and may play an important role in the
126 pathogenesis of ALS.
127
128

129 **Methods**

130 **Plasmids.** pEGFP-N1 vectors containing human $SOD1^{WT}$ and $SOD1^{A4V}$ were
131 generated as described [33]. GFP-Ub and mRFP-Ub (Addgene plasmids 11928 and
132 11935, provided by Nico Dantuma [31, 34]) were acquired from Addgene (USA). The
133 mcherry-Ub construct was created by replacing the mRFP sequence in mRFP-Ub with
134 mcherry fluorescent protein. The $tdTomato^{CL1}$ construct was obtained by cloning the
135 CL1 sequence (ACKNWFSSLSHFVIHL) into pcDNA3.1(+)tdTomato.

136

137 **Cell Culture and Transfection.** Neuroblastoma × Spinal cord hybrid NSC-34 cells
138 [35] were maintained in Dulbecco's Modified Eagles Medium/ Ham's Nutrient
139 Mixture F12 (DMEM/F12) supplemented with 10% foetal bovine serum (FBS,
140 Bovogen Biologicals, Australia). Cells were maintained at 37 °C in a humidified
141 incubator with 5% atmospheric CO_2. For confocal microscopy, cells were grown on
142 13 mm round coverslips in 24-well plates or on 8-well μ-slides (Ibidi, Germany).
143 Cells were grown in 6-well plates for cell lysate and cell sorting experiments. Cells
144 were transfected using Lipofectamine 3000 (Invitrogen, USA) according to
145 manufacturer's instructions with 0.5 μg DNA per well for a 24-well plate, 0.2 μg
146 DNA per well for 8-well μ-slides and 2.5 μg DNA per well for 6-well plates. For co-
147 transfections the amount of DNA was divided equally between constructs.

148

149 **Measurement of UPS function.** To quantify UPS activity, NSC-34 cells were co-
150 transfected with the fluorescent proteasome reporter $tdTomato^{CL1}$ and treated
151 overnight (~18 h) with 0-30μM of the proteasome inhibitor MG132. The level of
152 $tdTomato^{CL1}$ fluorescence was determined using flow cytometry on a Becton
153 Dickinson flow cytometer 48 h post transfection as in [36].

154

155 **Live cell imaging.** Imaging of NSC-34 cells co-transfected with SOD1^{A4V}-GFP and
156 mRFP-Ub was performed 24 h post transfection on a Leica TCS SP5 confocal
157 microscope. Cells were imaged every 15 min over 17 h in a CO_2 chamber maintained
158 at 37˚C with 5% CO_2. For fluorescence recovery after photobleaching (FRAP) and
159 fluorescence recovery after nucleus photobleaching (FRANP) experiments, analysis
160 was performed on transfected NSC-34 cells 48 h post transfection using the LAS AF
161 FRAP Application Wizard on the Leica TCS SP5 confocal Microscope. Images were
162 acquired using the 63× objective with two line averages and a scan speed of 700 Hz.
163 Five pre-bleach images were acquired over 7.5 s with the 561 nm laser set at 20%
164 power. The region of interest (ROI) was then bleached using the 'zoom in ROI'
165 method over five frames of 1.5 s at 100% laser power. For FRANP analysis, the entire
166 nucleus was bleached. Fluorescence recovery or loss was monitored for 120 s with the
167 laser power set back at 20%.

168

169 **Frequency distribution analysis.** GFP fluorescence in NSC-34 cells expressing
170 soluble and insoluble (aggregated) SOD1^{A4V}-GFP was quantified from confocal
171 images taken 48 h post transfection using ImageJ 1.48v [37]. Frequency distribution
172 analysis was subsequently performed in GraphPad Prism version 5.00 for Windows
173 (GraphPad software, USA).

174

175 **Immunofluorescence.** NSC-34 cells grown on coverslips were transfected with GFP-
176 tagged mutant SOD1 and fixed for 20 min at room temperature (RT) with 4%
177 paraformaldehyde (PFA) (Merck Millipore, USA) in phosphate buffered saline (PBS)
178 48 h post transfection. Cells were permeabilized in 1% tritonX-100 (TX-100) in PBS

179 for 30 min on ice before blocking for 1 h at RT with 5% FBS, 1% Bovine serum
180 albumin (BSA) 0.3% TX-100 in PBS. Cells were incubated with rabbit primary
181 antibodies against K48 or K63 Ub chain linkages (05-1307/05-1308, Merck
182 Millipore) overnight at 4 °C followed by Alexa Fluor 647-conjugated anti-rabbit IgG
183 secondary antibody for 5 h at RT. All antibodies were diluted in 1% BSA, 0.1% TX-
184 100 in PBS and cells were washed with PBS between each incubation step.
185
186 Spinal cord sections from the $SOD1^{G93A}$ mouse were also stained for SOD1 and K48
187 or K63 Ub chain linkages. A pap pen (Daido Sangyo, Tokyo, Japan) was used to
188 separate tissue sections mounted onto the same slide. Sections were then fixed with
189 4% PFA for 15 min at RT before permeabilization at RT for 10 min with 0.1% TX-
190 100 in PBS containing 2% (v/v) normal horse serum (NHS). Sections were then
191 blocked for 20 min at RT with 20% NHS and 2% BSA in PBS followed by staining
192 overnight at 4 °C in a humidified chamber with sheep anti-superoxide dismustase-1
193 (ab8866, Abcam, UK), mouse neuron-specific beta III tubulin antibody (ab78078,
194 Abcam) and rabbit anti-ubiquitin K48 or K63 (Merck, Millipore). The following day,
195 sections were incubated with Alexa Fluor-conjugated secondary antibodies reactive to
196 sheep, mouse and rabbit IgG for 1 h at RT. Following staining, coverslips were
197 mounted onto slides using ProLong Diamond Antifade Mountant (Molecular probes,
198 USA). All imaging experiments were analysed on a Leica TCS SP5 confocal
199 microscope.
200
201 **Cell lysis.** NSC-34 cells grown in 6-well plates and transfected with SOD1-GFP or
202 mRFP-Ub were harvested 48 h post transfection with trypsin/EDTA (Gibco, USA).
203 Cells were washed with PBS before being resuspended in RIPA buffer (50 mM

204 TrisHCl pH 7.4, 1% (w/v) sodium deoxycholate, 150 mM NaCl, 1 mM EDTA, 1%
205 TX-100, 0.1% SDS, 10mM NEM, 1 mM sodium orthovanadate, Halt™ Protease
206 Inhibitor Cocktail (Thermo Scientific, USA)). Protein concentration was determined
207 by BCA assay.
208
209 **Western blot.** Cell lysates with a total protein concentration of 100 µg were reduced
210 with β-mercaptoethanol and heated for 10 min at 70 °C before being analysed on a
211 Mini-PROTEAN TGX Stain-Free Gel (Bio-Rad, USA) for 2 h at 100 V. Proteins
212 were transferred onto a nitrocellulose membrane (Pall Corporation, USA) using the
213 standard protocol on the Bio-Rad Trans-Blot Turbo Transfer System. The membrane
214 was blocked in 5% skim milk powder in Tris buffered saline, 0.2% (v/v) Tween-20
215 (TBST) for 1 h at RT before probing for Ub with rabbit anti-ubiquitin antibody
216 (ab137025, Abcam) overnight at 4 °C. The following day the membrane was washed
217 three times with TBST over 30 min before incubating with horseradish peroxidise-
218 conjugated anti-rabbit antibody (1706515, Bio-Rad) for 1 h at RT. The membrane was
219 visualised with chemiluminescent substrate (Thermo Scientific) on the Amersham
220 Imager 6600RGB.
221
222 **Cell sorting.** NSC-34 cells transfected with SOD1-GFP were harvested 48 h post-
223 transfection with trypsin-EDTA (Gibco) and washed with PBS before being
224 resuspended in resuspension buffer (PBS containing 25 mM HEPES, 1 mM EDTA
225 and 1% FBS) and filtered through a 40 µm nylon mesh strainer (Greiner Bio-One,
226 Austria). Enrichment of GFP positive cells was performed on a Bio-Rad S3e cell
227 sorter. Cells were sorted based on GFP fluorescence (excitation 488 nm, emission
228 525/30nm) and collected into 5 mL FACS tubes containing DMEM/F12

229 supplemented with 10% FBS and 2 × penicillin/streptomycin (Gibco). Following
230 enrichment, cells were lysed in RIPA buffer (as above) for ubiquitomics analysis.
231
232 **Ubiquitomics.** Proteomics to identify ubiquitin-modified proteome (ubiquitome) in
233 NSC-34 cells was performed as described in [38]. Cells were lysed in lysis buffer (50
234 mM Tris-HCl (pH 7.5), 150 mM NaCl, 0.5% NP-40, 1 mM DTT, 1× EDTA-free
235 protease inhibitor cocktail, 10 mM N-ethylmaleimide, 1 mM sodium orthovanadate).
236 Protein concentration was determined using a BCA assay and 300 µg of total protein
237 was used per sample to immunopurify mono- and poly-ubiquitinated proteins using
238 30 µL of VIVAbind Ub affinity matrix (Ubiquitin Kit, VIVA Bioscience). Samples
239 were incubated for 2 h at 4 °C with end-to-end mixing then matrix was collected by
240 centrifugation (1 min; 4 °C; 1000 × g) and washed six times in detergent free wash
241 buffer (500 µL). After washing, beads were digested for 30 min at 27 °C, then
242 reduced with 1 mM DTT and left to digest overnight at room temperature with
243 sequencing-grade trypsin (5 µg/mL, Promega), as described previously [39]. Samples
244 were alkylated with 5 mg/mL iodoacetamide and protease digestion terminated with
245 trifluoroacetic acid. Trypsinized eluents were collected after brief centrifugation then
246 purified and desalted using self-packed tips with 6 layers of C18 Empore disks
247 (Pacific Laboratory Products), then dried in a SpeedVac. Samples were then
248 resuspended in 12 µL 5% formic acid, 2% acetonitrile and stored at -80 °C.
249 For nLC-MS/MS analysis, 5 uL of each of the peptide samples were loaded and
250 separated along a C18 column (400 mm, 75 µm ID, 3 µm silica beads) and introduced
251 by nanoelectrospray into an LTQ Orbitrap Velos Pro coupled to an Easy-nLC HPLC
252 (Thermo Fisher). Tandem mass spectrometry data was collected for the top 10 most
253 abundant ions per scan over a 140-minute time gradient. The order of data collection

254 was randomized to interchange between biological conditions with BSA run between
255 each sample to minimize temporal bias. MS/MS raw files were analyzed using the
256 Andromeda search engine integrated into MaxQuant (v1.2.7.4) [40] against the
257 Uniprot Mouse database. A false discovery rate of 1% was tolerated for protein,
258 peptide, and sites, and one missed cleavage was allowed. MaxQuant output data were
259 filtered to remove contaminants, reverse hits, proteins only identified by site and
260 proteins with < 2 unique peptides [41]. An individual protein was defined as present
261 under a particular condition if it was detected in a minimum of two replicates.
262 Protein-protein interactions and KEGG pathway analysis among the resulting protein
263 list was analyzed using STRING (v10) [42] (with a confidence score of 0.700) and
264 Cytoscape (v3.1.1) [43].
265
266 **Analysis of Mitochondrial Morphology and Function.** NSC-34 cells transiently
267 transfected with SOD1-GFP were incubated with 100nM Mitotracker Deep Red FM
268 (Molecular probes) or Mitotracker CMXRos (Molecular probes) for 30 min at 37 °C
269 prior to analysis by confocal microscopy or flow cytometry 48 h post transfection.
270 Mitochondrial morphology was examined using a mitochondrial morphology macro
271 [44] on ImageJ 1.48v. Mitotracker Red and Mitotracker CMXRos accumulation in
272 cells expressing high levels of SOD1-GFP was also assessed by flow cytometry
273 (Becton Dickinson).
274
275

276 **Results**

277 **SOD1 aggregates are ubiquitylated early**

278 We previously showed that all cellular SOD1 aggregates contained Ub at the time
279 points tested [45]. Here we used real-time imaging using a Ub fusion protein to follow
280 inclusion formation in a single cell from its genesis until it had taken up a large
281 proportion of the cytoplasm. Previous work has demonstrated that the behaviour of
282 GFP-Ub fusions in cells is indistinguishable from endogenous Ub and provides a
283 robust fluorescent indicator of Ub distribution [31]. We created a mCherry-Ub fusion
284 protein that behaved in a similar manner to the GFP fusion protein (supplementary
285 **Figure S1**). Ub was observed in foci at the earliest detectable stages of SOD1
286 aggregation (**Figure 2A**, see insert). Ub was continuously added to inclusions
287 throughout their formation, as was SOD1 (**Figure 2A**). To ensure that the Ub
288 accumulation in SOD1 inclusions was not an artefact of Ub over expression, we next
289 probed for endogenous Ub using antibodies. $SOD1^{A4V}$ expression causes inclusions in
290 approximately 15% of NSC-34 cells (**Figure S2)** and in those cells that contain
291 inclusions we observed a high degree of overlap between SOD1 aggregates and Ub
292 when using both K48 and K63 chain specific antibodies (**Figure 2B**). We also found
293 that SOD1 aggregates contained K48 chains in $SOD1^{G93A}$ mouse spinal motor
294 neurons (**Figure 2C**).

295

296 **Cells with SOD1 aggregates have increased UPS dysfunction**

297 We previously showed that a UPS reporter containing a CL1 degron peptide for rapid
298 degradation accumulates to significantly higher amounts in ALS patient fibroblasts
299 compared to controls, suggesting an overwhelmed UPS [36]. Work from others
300 suggests that SOD1 aggregates are toxic because they interfere with the quality

301 control function of the juxtanuclear quality control compartment (JUNQ) [20]. To
302 examine the relationship between SOD1 aggregation and UPS dysfunction we used
303 transiently transfected NSC-34 cells that contained SOD1^{A4V}-GFP and tdTomato^{CL1}.
304 We initially used flow cytometry to examine the effect of proteasome inhibition on
305 reporter accumulation. While there was a significant difference in reporter signal
306 between SOD1 and SOD1^{A4V} expressing cells, both cell lines showed a similar dose-
307 dependent increase in reporter signal with MG132 treatment (**Figure 3A**). This
308 suggests that, while SOD1 ^{A4V} expression causes significant UPS disruption, there is
309 no specific vulnerability to proteasome inhibition of cells expressing mutant SOD1
310 compared to wild-type expressing cells.
311
312 However, this analysis examined the entire population of SOD1^{WT} or SOD1^{A4V}
313 expressing cells and previous work using a similar CL1-containing fluorescent
314 reporter suggests that the aggregation of Huntingtin and CFTR cause UPS
315 dysfunction [46]. We hypothesized that inclusions formed by mutant SOD1 might
316 influence UPS activity in a similar fashion, a phenomenon that may not be observed
317 when analysing the entire population of cells, given that only 15% of NSC-34 cells
318 expressing SOD1^{A4V} produce inclusions (**Figure S2**). In order to identify cells with
319 SOD1 inclusions in our flow cytometry data we tested the relationship between
320 aggregation and total cellular fluorescence (**Figure 3B**). Cells were transiently
321 transfected with SOD1^{A4V}-GFP and imaged 48 h post transfection using confocal
322 microscopy. The total cellular fluorescence for individual cells was plotted for both
323 cells with and without inclusions. The fluorescence of both populations was normally
324 distributed (**Figure 3B**). The mean fluorescence of cells containing aggregates was
325 significantly greater than that of cells without aggregates (**Figure 3C**), presumably

326 due to continued accumulation of SOD1 into inclusions. However, there was
327 significant overlap between the two populations so we could not distinguish
328 populations entirely. We decided to analyze the most highly fluorescent cells (top
329 10%) across the entire population. In this subset of cells, approximately 80%
330 contained $SOD1^{A4V}$ inclusions (**Figure 3D**). We reasoned that analyzing the top 10%
331 fluorescent cells would sufficiently enrich for cells containing inclusions. Using flow
332 cytometry, we observed a 4× increase in reporter fluorescence ($P< 0.001$) - indicating
333 UPS dysfunction - in the top 10% of $SOD1^{A4V}$–GFP expressing cells compared to
334 control cells in the same fluorescence range. That is, UPS dysfunction in $SOD1^{A4V}$
335 cells is largely restricted to cells containing aggregates. By comparison, only a small
336 increase (1.2×) in reporter fluorescence was observed in the entire population of
337 $SOD1^{A4V}$–GFP expressing cells compared with the entire $SOD1^{WT}$-GFP expressing
338 population ($P< 0.01$) (**Figure 3E**). This suggests that SOD1 aggregation is associated
339 with compromised UPS function.
340
341 **Ubiquitin pools are disturbed in cells containing SOD1 aggregates**
342 Ub exists in a dynamic equilibrium in the cell, partitioning into four major pools; i)
343 immobile in the nucleus, ii) immobile in the cytoplasm, iii) soluble polyUb chains and
344 iv) a small fraction as free monomeric Ub [31]. Mobile Ub is a combination of free
345 monomeric Ub, free Ub chains and Ub attached to diffusible proteins (**Figure 1**).
346 Immobile Ub is primarily bound to histones in the nucleus and bound to organelles
347 and cytoskeleton in the cytoplasm (**Figure 1**). To determine if the observed UPS
348 dysfunction in cells with mutant SOD1 aggregates was associated with altered Ub
349 homeostasis we examined the relative distribution of Ub into different cellular pools
350 following expression of wild-type or mutant SOD1 genes by FRAP (**Figure 4A-E**).

351 The diffusion rate back into the bleached area provides information on the mobility of
352 the Ub species present in solution and the amount of immobile fluorophore in the
353 compartment of interest (i.e. bound to membrane vesicles or cytoskeleton in the
354 cytosol, and bound to histones in the nucleus). We selected ROIs in both the nucleus
355 and cytoplasm (**Figure 4B**) in cells co-expressing mCherry-Ub and either GFP,
356 $SOD1^{WT}$-GFP or SOD^{A4V}-GFP. In the case of SOD^{A4V}-GFP expressing cells, we
357 performed the analysis on two subpopulations, with and without aggregates. As
358 previously reported, we find that Ub fluorescence recovery after bleaching (indicating
359 Ub mobility) is higher in the cytoplasm than in the nucleus, likely due to a large
360 proportion of nuclear Ub being attached to histones. Patterns of recovery appeared
361 similar in all treatments, with the exception of a lower cytoplasmic recovery in the
362 cells containing SOD^{A4V}-GFP aggregates (**Figure 4A**). After calculating the mean
363 half-life ($T_{1/2}$) of recovery in each case, we find no significant differences between
364 any of the cell populations (**Figure 4D**). This suggests that within the mobile
365 population of Ub, the presence of SOD^{A4V}-GFP aggregates does not significantly alter
366 the kinetics of Ub diffusion.
367
368 This observation prompted us to investigate whether SOD^{A4V}-GFP aggregates alter
369 the amount of mobile Ub available in the cell. We find that on average, 51% of the
370 cellular Ub signal is detected in aggregates, indicating that the presence of insoluble
371 aggregates alters the distribution of the Ub pool (**Figure 4C**). The significance of this
372 aggregate-associated fraction of Ub is clear in the context of our analysis of the
373 relative distribution of mobile Ub pools. Based on our FRAP analysis, which does not
374 consider the aggregate-associated Ub, there is no significant difference in the mobility
375 of Ub between SOD^{A4V}-GFP cells and controls (**Figure 4E**). However, if we correct

376 for the 51% of Ub we know to be immobile in cells with inclusions, we find that the
377 actual mobile Ub pool in SOD^{A4V}-GFP cells is significantly smaller than in controls
378 (**Figure 4E**).
379
380 **Free monomeric ubiquitin is lowered in cells with SOD1 aggregates**
381 To test whether the depletion of mobile Ub in cells containing SOD^{A4V}-GFP
382 aggregates may diminish free monomeric Ub, we next examined the relative amounts
383 of monomeric Ub in cells expressing GFP, $SOD1^{WT}$-GFP, or SOD^{A4V}-GFP for 48 h,
384 by Western blot (**Figure 5A**). We did not observe any significant differences using
385 this method, likely due to the fact that this analysis represents a total measure of all
386 cells in the culture, including non-transfected cells. We therefore turned to
387 fluorescence recovery after nucleus photobleaching (FRANP) analysis to monitor free
388 Ub in single cells. Monomeric mCherry-Ub will diffuse through the nuclear pore (<
389 60 kDa), while mCherry-Ub incorporated into Ub chains will not [31]. Hence, relative
390 free monomeric Ub can be measured by monitoring diffusion through the nuclear pore
391 following fluorescence bleaching solely in the nucleus or cytosol [31]. We transfected
392 cells with GFP, $SOD1^{WT}$-GFP, or SOD^{A4V}-GFP (**Figure 5B**) for 48 h, then bleached
393 the entire nucleus and quantified the amount of relative monomeric Ub diffusing
394 through the nuclear pore back into the nucleus (**Figure 5C**). We observed a
395 significant drop in free monomeric Ub in cells containing SOD^{A4V}-GFP aggregates,
396 but no difference in the level of monomeric Ub between cells expressing $SOD1^{WT}$ and
397 SOD^{A4V} in the absence of inclusions (**Figure 5D**).
398
399 **SOD^{A4V}-GFP induced changes in the ubiquitome of NSC34 cells**

400 Free Ub exists in complex equilibrium with multiple conjugated forms and ALS
401 mutations may induce redistribution of Ub through altered activity in various cellular
402 pathways. To investigate changes in the Ub-modified proteome (ubiquitome) of cells
403 expressing SOD^{WT} compared with SOD^{A4V}-GFP, we performed proteomics following
404 enrichment of cell lysates for ubiquitylated proteins (**Figure 6A**). We identified 316
405 ubiquitylated proteins common to cells expressing either wild-type or mutant SOD1.
406 55 proteins were uniquely present in the ubiquitome of cells expressing mutant SOD1
407 and 12 unique proteins were identified in the ubiquitome of cells expressing wild-type
408 SOD1 (**Figure 6B, and Table 1**). Network analysis of known protein-protein
409 interactions and ontology in the set of ubiquitylated proteins unique to cell expressing
410 mutant SOD1 using the String database [42] identified a number of enriched
411 pathways, including metabolic pathways, ubiquitin-proteasome system (UPS),
412 ribosome and mRNA processing and transport (**Figure 6C**). Expression of a chronic
413 misfolded protein has previously been observed to increase proteome misfolding and
414 we have shown that ALS aggregates are composed of supersaturated proteins - that is,
415 proteins which have expression levels higher than one might predict given their
416 solubility [5].
417
418 We compared the supersaturation scores for both the unfolded and native states of
419 ubiquitylated proteins found uniquely in SOD^{A4V}-GFP expressing cells to the whole
420 proteome. The median supersaturation score of these 55 ubiquitylated proteins is 10 ×
421 higher than the whole proteome in the unfolded state ($\boldsymbol{\sigma}_u$) and 25 x higher than the
422 whole proteome in the native state ($\boldsymbol{\sigma}_f$) (**Figure 6D**). These data are consistent with
423 proteome instability and resulting redeployment of Ub driving altered Ub distribution

424 and subsequent impairment of Ub homeostasis upon expression of a chronically
425 misfolded protein.

426 **Cells with SOD1 aggregates have altered mitochondrial morphology and**
427 **function**

428 Pathway analysis of our ubiquitome data (above) indicated specific enrichment of
429 mitochondrial/metabolic proteins in the ubiquitome of $SOD1^{A4V}$-expressing cells
430 (**Table 1**), suggesting that Ub redistribution/homeostasis might be associated with
431 compromised mitochondrial function in these cells. Indeed, previous work has shown
432 that mutations in SOD1 lead to mitochondrial dysfunction [47-49]. In order to assess
433 mitochondrial function in $SOD1^{A4V}$-expressing cells, we first examined mitochondrial
434 morphology using Mitotracker and confocal microscopy (**Figure 7A-C**). We found
435 that $SOD1^{A4V}$-expressing cells contained a significantly higher number of
436 mitochondria per cell compared to controls (**Figure 7B**). In addition, we these
437 mitochondria are significantly more circular than those in control cells (**Figure 7C**).
438 We quantified mitotracker fluorescence in cells using flow cytometry, as above
439 focusing on the top 10% most fluorescent cells (based on SOD-GFP expression) to
440 enrich for cells with aggregates (i.e. when expressing $SOD1^{A4V}$). This subset of
441 $SOD1^{A4V}$-expressing cells has higher mitotracker fluorescence compared to $SOD1^{WT}$
442 expressing cells exhibiting the same level of fluorescence - consistent with
443 accumulation of mitochondria with $SOD1^{A4V}$ expression (**Figure 7D**). In the same
444 subset of aggregate-containing cells we observed increased fluorescence of the
445 functional reporter CMXRos, suggesting alterations in mitochondrial membrane
446 potential (**Figure 7E**).

447

448

449

450 **Discussion**

451 A unifying feature of neurodegenerative diseases such as ALS is the presence of Ub
452 within insoluble protein aggregates [10, 50, 51]. Beyond labelling substrates for
453 degradation via the proteasome, Ub is an important regulator of cellular processes
454 such as transcription, translation, endocytosis and DNA repair. The sequestration of
455 Ub into inclusions may therefore reduce the availability of free Ub essential for these
456 processes, compromising cellular function and survival. To gain insight into the
457 regulation of Ub homeostasis in ALS, we followed the dynamic distribution of Ub at
458 a single cell level in a well-established SOD1 cell model of ALS. Our results confirm
459 that the expression of mutant SOD1 leads to UPS dysfunction and corresponding
460 disruption of Ub homeostasis, suggesting these processes plays a key role in the
461 development of ALS pathology.

462

463 In cell models, Ub regulates the concentrations of TDP-43 and SOD1 [52, 53], and
464 proteasome inhibition can trigger their abnormal accumulation. While our previous
465 work established that SOD1 aggregates contain Ub [45], results here confirm that
466 SOD1 co-aggregates with Ub, and that Ub is present at the earliest stage of
467 aggregation. Furthermore, SOD1 aggregates were found to contain both K48 and K63
468 polyubiquitin chains, signalling degradation via the proteasome and autophagy
469 pathways, respectively. Interestingly, both K48 and K63-linked ubiquitylation has
470 been associated with the formation of inclusions [54], with previous studies showing
471 that K63 polyubiquitination directs misfolded SOD1 to the ubiquitin-aggresome route
472 when the UPS is inhibited [55]. These data are consistent with the need for tightly
473 regulated Ub homeostasis in neurons, and suggest any perturbation in this
474 homeostasis could cause Ub depletion and subsequent toxicity. It is likely that protein

475 aggregation causes Ub depletion, which could then drive further aggregation in a
476 positive feedback loop (**Figure 8**).
477
478 In the nervous system, the UPS contributes to the regulation of many aspects of
479 synaptic function, such as neuronal growth and development, neuronal excitability,
480 neurotransmission, long-term potentiation (LTP) and synapse formation and
481 elimination [56, 57]. UPS dysfunction is therefore central to neuronal health and
482 neurodegenerative disease [6]. Impairment of the UPS has been implicated strongly in
483 the pathogenesis of ALS [52, 58, 59]. Here, we reveal that the aggregation of SOD1
484 compromises UPS function, decreasing cellular capacity to degrade the proteasome
485 reporter tdTomato^{CL1}. Our findings are consistent with the previous demonstration of
486 UPS dysfunction in ALS, with accumulation of the fluorescent UPS reporter Ub^{G76V}-
487 GFP observed in the spinal cord and cranial motor neurons of SOD1^{G93A} mice [59].
488 Moreover, a motor neuron specific knockdown of proteasome subunit Rpt3 in the
489 absence of ALS genetic background results in an ALS phenotype in mice - including
490 locomotor dysfunction, progressive motor neuron loss and mislocalization of ALS
491 markers TDP-43, FUS, ubiquilin 2, and optineurin [58]. These data support a model
492 where a reduction in UPS capacity is sufficient to drive ALS pathology in mice. Not
493 even overexpression of human mutant TDP-43 gives such an accurate reproduction of
494 a human ALS-like phenotype in mice. In ALS patient spinal motor neurons, 85%
495 (38/40) of cytoplasmic TDP-43 foci or inclusions were positive for Ub. In fact, almost
496 all cellular Ub in these neurons was sequestered within large, skein-like inclusions
497 [45]. Interestingly, Ub has been found to accumulate in inclusions without the
498 aggregation of TDP-43 in sporadic ALS [7], suggesting that aggregation of proteins
499 such as TDP-43, FUS and SOD1 may not be necessary for Ub depletion-induced

500 toxicity. In human skin fibroblasts it has been shown that the UPS reporter GFP^{CL1}
501 accumulates significantly more in ALS patient fibroblasts compared to controls,
502 suggesting a compromised UPS [36]. This raises the question of whether there are
503 alternate means to control protein concentration when protein aggregates disrupt
504 degradation mechanisms. It was recently proposed that widespread transcriptional
505 repression may serve this purpose in Alzheimer's disease [60].
506
507 The work presented here suggests that the aggregation of misfolded SOD1 alters Ub
508 homeostasis and subsequently depletes the free Ub pool in cells. Cellular Ub exists in
509 a complex equilibrium between free and conjugated Ub [31]. Neurons are vulnerable
510 to free Ub deficiency, which if prolonged may lead to cell death [61, 62]. Many
511 factors can influence Ub homeostasis. For example, proteasome inhibition depletes
512 free Ub to as low as 5% of basal levels in less than 2 h [63, 64]. Inhibition of
513 translation also depletes free Ub through reduced production, while toxicity can be
514 rescued by overexpression of Ub [65]. Accumulation of ubiquitylated proteins in
515 inclusions is an important potential mechanism for depletion of free Ub, and in this
516 context free Ub levels can be partially restored by overexpression or removal of Ub
517 from the aggregated protein through ubiquitin-specific proteases. It was recently
518 shown that while the ataxia associated mutation in Usp14 causes reduction in free Ub
519 and neuromuscular junction dysfunction in mice, overexpression of Ub restored free
520 Ub levels in motor neurons and improved NMJ structure [66]. Additionally, free Ub
521 could be increased in cells containing huntingtin aggregates by overexpression of the
522 de-ubiquitylation enzyme USP14 [67]. Not only did this protect cells from aggregate-
523 induced toxicity, it also reduced ER stress, which is thought to precede inclusion
524 formation in ALS models [18]. These data further support the concept that modulation

525 of cellular Ub pools is an important factor in the pathogenesis of neurodegenerative
526 disease.
527
528 The pathways responsible for modulating Ub homeostasis in ALS are not yet well
529 understood. Our ubiquitomics analysis of cells expressing SOD1 reveals that the
530 unique ubiquitome of cells expressing mutant SOD1 is enriched for proteins prone to
531 aggregation (i.e. supersaturated). This is consistent with findings that proteins
532 associated with neurodegeneration are supersaturated [5, 25, 26]. Furthermore, a
533 substantial proportion of the ubiquitylated proteins identified are from pathways
534 known to be dysfunctional in ALS, including RNA processing, metabolic and
535 mitochondrial pathways. This is not surprising given that both RNA binding proteins
536 and oxidative phosphorylation and metabolic pathways are also prone to aggregation
537 in neurodegeneration [26]. These results suggest that mutations in SOD1 may lead to
538 mitochondrial dysfunction by disrupting Ub homeostasis. Interestingly, we find that
539 cells expressing mutant SOD1 had altered mitochondrial morphology and function.
540 Disturbances to mitochondrial morphology have been previously reported in human
541 motor neurons carrying the $SOD1^{A4V}$ mutation [68] and recent studies have revealed
542 that mitochondrial impairment occurs soon after proteasome inhibition [69]. In fact,
543 continued proteasome dysfunction in mouse brain cortical neurons inhibited the
544 degradation of ubiquitylated mitochondrial proteins and led to the accumulation of
545 dysfunctional mitochondria [70]. Misfolded proteins such as mutant SOD1 have also
546 been shown to interact with mitochondrial proteins and translocate into the
547 mitochondrial matrix, where they accumulate and induce mitochondrial dysfunction
548 [71-73]. However, this cytotoxicity can be attenuated through the ubiquitylation of
549 misfolded but non-aggregated SOD1 - which promotes its degradation via the UPS

550 [74]. Collectively, these studies demonstrate an integral functional relationship
551 between impairment of the UPS and mitochondrial dysfunction, and that modulation
552 of cellular Ub pools may rescue mitochondrial dysfunction caused by the
553 accumulation of SOD1.
554
555 **Conclusions**
556 In conclusion, we observe that the aggregation of mutant SOD1 leads to altered UPS
557 activity and redistribution of Ub, causing disrupted Ub homeostasis. Given that Ub
558 controls many essential cellular pathways that are also dysfunctional in ALS -
559 including transcription, translation, vesicle transport, mitochondrial function and
560 apoptosis - these findings suggest that Ub homeostasis is a central feature of ALS
561 pathogenesis. Further understanding of the contribution of Ub homeostasis to ALS
562 pathology may be imperative to understanding the molecular pathways underpinning
563 neurodegenerative disease more broadly.
564
565
566

567 **List of abbreviations**
568 Amyotrophic lateral sclerosis (ALS)
569 Bovine serum albumin (BSA)
570 Deubiquitinating enzymes (DUBS)
571 Familial ALS (fALS)
572 Fluorescence loss in photobleaching (FLIP)
573 Fluorescence recovery after photobleaching (FRAP)
574 Frontotemporal dementia (FTD)
575 Juxtanuclear quality control compartment (JUNQ)
576 Long-term potentiation (LTP)
577 Motor neuron disease (MND)
578 Neuromuscular junction (NMJ)
579 Paraformaldehyde (PFA)
580 Phosphate buffered saline (PBS)
581 Region of interest (ROI)
582 Room temperature (RT)
583 Sporadic ALS (sALS)
584 Superoxide dismutase 1 (SOD1)
585 TritonX-100 (TX-100)
586 Ubiquitin (Ub)
587 Ubiquitin-proteasome system (UPS)
588
589
590
591
592

References

[1] M.R. Turner, O. Hardiman, M. Benatar, B.R. Brooks, A. Chio, M. de Carvalho, P.G. Ince, C. Lin, R.G. Miller, H. Mitsumoto, G. Nicholson, J. Ravits, P.J. Shaw, M. Swash, K. Talbot, B.J. Traynor, L.H. Van den Berg, J.H. Veldink, S. Vucic, M.C. Kiernan, Controversies and priorities in amyotrophic lateral sclerosis, Lancet Neurol 12(3) (2013) 310-22.

[2] S. Chen, P. Sayana, X. Zhang, W. Le, Genetics of amyotrophic lateral sclerosis: an update, Mol Neurodegener 8 (2013) 28.

[3] E.T. Cirulli, B.N. Lasseigne, S. Petrovski, P.C. Sapp, P.A. Dion, C.S. Leblond, J. Couthouis, Y.F. Lu, Q. Wang, B.J. Krueger, Z. Ren, J. Keebler, Y. Han, S.E. Levy, B.E. Boone, J.R. Wimbish, L.L. Waite, A.L. Jones, J.P. Carulli, A.G. Day-Williams, J.F. Staropoli, W.W. Xin, A. Chesi, A.R. Raphael, D. McKenna-Yasek, J. Cady, J.M. Vianney de Jong, K.P. Kenna, B.N. Smith, S. Topp, J. Miller, A. Gkazi, F.S. Consortium, A. Al-Chalabi, L.H. van den Berg, J. Veldink, V. Silani, N. Ticozzi, C.E. Shaw, R.H. Baloh, S. Appel, E. Simpson, C. Lagier-Tourenne, S.M. Pulst, S. Gibson, J.Q. Trojanowski, L. Elman, L. McCluskey, M. Grossman, N.A. Shneider, W.K. Chung, J.M. Ravits, J.D. Glass, K.B. Sims, V.M. Van Deerlin, T. Maniatis, S.D. Hayes, A. Ordureau, S. Swarup, J. Landers, F. Baas, A.S. Allen, R.S. Bedlack, J.W. Harper, A.D. Gitler, G.A. Rouleau, R. Brown, M.B. Harms, G.M. Cooper, T. Harris, R.M. Myers, D.B. Goldstein, Exome sequencing in amyotrophic lateral sclerosis identifies risk genes and pathways, Science (2015).

[4] K.L. Williams, S. Topp, S. Yang, B. Smith, J.A. Fifita, S.T. Warraich, K.Y. Zhang, N. Farrawell, C. Vance, X. Hu, A. Chesi, C.S. Leblond, A. Lee, S.L. Rayner, V. Sundaramoorthy, C. Dobson-Stone, M.P. Molloy, M. van Blitterswijk, D.W. Dickson, R.C. Petersen, N.R. Graff-Radford, B.F. Boeve, M.E. Murray, C. Pottier, E. Don, C. Winnick, E.P. McCann, A. Hogan, H. Daoud, A. Levert, P.A. Dion, J. Mitsui, H. Ishiura, Y. Takahashi, J. Goto, J. Kost, C. Gellera, A.S. Gkazi, J. Miller, J. Stockton, W.S. Brooks, K. Boundy, M. Polak, J.L. Munoz-Blanco, J. Esteban-Perez, A. Rabano, O. Hardiman, K.E. Morrison, N. Ticozzi, V. Silani, J. de Belleroche, J.D. Glass, J.B. Kwok, G.J. Guillemin, R.S. Chung, S. Tsuji, R.H. Brown, Jr., A. Garcia-Redondo, R. Rademakers, J.E. Landers, A.D. Gitler, G.A. Rouleau, N.J. Cole, J.J. Yerbury, J.D. Atkin, C.E. Shaw, G.A. Nicholson, I.P. Blair, CCNF mutations in amyotrophic lateral sclerosis and frontotemporal dementia, Nat Commun 7 (2016) 11253.

[5] P. Ciryam, I.A. Lambert-Smith, D.M. Bean, R. Freer, F. Cid, G.G. Tartaglia, D.N. Saunders, M.R. Wilson, S.G. Oliver, R.I. Morimoto, C.M. Dobson, M. Vendruscolo, G. Favrin, J.J. Yerbury, Spinal motor neuron protein supersaturation patterns are associated with inclusion body formation in ALS, Proc Natl Acad Sci U S A (2017).

[6] J.J. Yerbury, L. Ooi, A. Dillin, D.N. Saunders, D.M. Hatters, P.M. Beart, N.R. Cashman, M.R. Wilson, H. Ecroyd, Walking the tightrope: proteostasis and neurodegenerative disease, J Neurochem 137(4) (2016) 489-505.

[7] M.T. Giordana, M. Piccinini, S. Grifoni, G. De Marco, M. Vercellino, M. Magistrello, A. Pellerino, B. Buccinna, E. Lupino, M.T. Rinaudo, TDP-43 redistribution is an early event in sporadic amyotrophic lateral sclerosis, Brain Pathol 20(2) (2010) 351-60.

[8] J. Brettschneider, K. Arai, K. Del Tredici, J.B. Toledo, J.L. Robinson, E.B. Lee, S. Kuwabara, K. Shibuya, D.J. Irwin, L. Fang, V.M. Van Deerlin, L. Elman, L. McCluskey, A.C. Ludolph, V.M. Lee, H. Braak, J.Q. Trojanowski, TDP-43 pathology

642 and neuronal loss in amyotrophic lateral sclerosis spinal cord, Acta Neuropathol
643 128(3) (2014) 423-37.
644 [9] N. Ticozzi, A. Ratti, V. Silani, Protein aggregation and defective RNA
645 metabolism as mechanisms for motor neuron damage, CNS and Neurological
646 Disorders - Drug Targets 9(3) (2010) 285-296.
647 [10] P.N. Leigh, H. Whitwell, O. Garofalo, J. Buller, M. Swash, J.E. Martin, J.M. Gallo,
648 R.O. Weller, B.H. Anderton, Ubiquitin-immunoreactive intraneuronal inclusions
649 in amyotrophic lateral sclerosis. Morphology, distribution, and specificity, Brain
650 114(2) (1991) 775-788.
651 [11] M.J. Strong, S. Kesavapany, H.C. Pant, The pathobiology of amyotrophic
652 lateral sclerosis: A proteinopathy?, Journal of Neuropathology and Experimental
653 Neurology 64(8) (2005) 649-664.
654 [12] L. McAlary, J.A. Aquilina, J.J. Yerbury, Susceptibility of Mutant SOD1 to Form
655 a Destabilized Monomer Predicts Cellular Aggregation and Toxicity but Not In
656 vitro Aggregation Propensity, Front Neurosci 10 (2016) 499.
657 [13] R. Zeineddine, J.F. Pundavela, L. Corcoran, E.M. Stewart, D. Do-Ha, M. Bax, G.
658 Guillemin, K.L. Vine, D.M. Hatters, H. Ecroyd, C.M. Dobson, B.J. Turner, L. Ooi, M.R.
659 Wilson, N.R. Cashman, J.J. Yerbury, SOD1 protein aggregates stimulate
660 macropinocytosis in neurons to facilitate their propagation, Mol Neurodegener
661 10 (2015) 57.
662 [14] C. Munch, J. O'Brien, A. Bertolotti, Prion-like propagation of mutant
663 superoxide dismutase-1 misfolding in neuronal cells, Proc Natl Acad Sci U S A
664 108(9) (2011) 3548-53.
665 [15] V. Sundaramoorthy, A.K. Walker, J. Yerbury, K.Y. Soo, M.A. Farg, V. Hoang, R.
666 Zeineddine, D. Spencer, J.D. Atkin, Extracellular wildtype and mutant SOD1
667 induces ER-Golgi pathology characteristic of amyotrophic lateral sclerosis in
668 neuronal cells, Cell Mol Life Sci 70(21) (2013) 4181-95.
669 [16] L.I. Grad, J.J. Yerbury, B.J. Turner, W.C. Guest, E. Pokrishevsky, M.A. O'Neill, A.
670 Yanai, J.M. Silverman, R. Zeineddine, L. Corcoran, J.R. Kumita, L.M. Luheshi, M.
671 Yousefi, B.M. Coleman, A.F. Hill, S.S. Plotkin, I.R. Mackenzie, N.R. Cashman,
672 Intercellular propagated misfolding of wild-type Cu/Zn superoxide dismutase
673 occurs via exosome-dependent and -independent mechanisms, Proc Natl Acad
674 Sci U S A 111(9) (2014) 3620-5.
675 [17] L. McAlary, J.J. Yerbury, J.A. Aquilina, Glutathionylation potentiates benign
676 superoxide dismutase 1 variants to the toxic forms associated with amyotrophic
677 lateral sclerosis, Sci Rep 3 (2013) 3275.
678 [18] J.D. Atkin, M.A. Farg, K.Y. Soo, A.K. Walker, M. Halloran, B.J. Turner, P. Nagley,
679 M.K. Horne, Mutant SOD1 inhibits ER-Golgi transport in amyotrophic lateral
680 sclerosis, J Neurochem 129(1) (2014) 190-204.
681 [19] A.S. Tsvetkov, M. Arrasate, S. Barmada, D.M. Ando, P. Sharma, B.A. Shaby, S.
682 Finkbeiner, Proteostasis of polyglutamine varies among neurons and predicts
683 neurodegeneration, Nat Chem Biol 9(9) (2013) 586-92.
684 [20] S.J. Weisberg, R. Lyakhovetsky, A.C. Werdiger, A.D. Gitler, Y. Soen, D.
685 Kaganovich, Compartmentalization of superoxide dismutase 1 (SOD1G93A)
686 aggregates determines their toxicity, Proc Natl Acad Sci U S A 109(39) (2012)
687 15811-6.
688 [21] F. Chiti, C.M. Dobson, Protein misfolding, functional amyloid, and human
689 disease, Annu Rev Biochem 75 (2006) 333-66.

690 [22] M.Y. Sherman, A.L. Goldberg, Cellular defenses against unfolded proteins: a
691 cell biologist thinks about neurodegenerative diseases, Neuron 29(1) (2001) 15-
692 32.
693 [23] J.J. Yerbury, J.R. Kumita, Protein chemistry of amyloid fibrils and
694 chaperones: Implications for amyloid formation and disease, Current Chemical
695 Biology 4(2) (2010) 89-98.
696 [24] Q. Huang, M.E. Figueiredo-Pereira, Ubiquitin/proteasome pathway
697 impairment in neurodegeneration: Therapeutic implications, Apoptosis 15(11)
698 (2010) 1292-1311.
699 [25] P. Ciryam, G.G. Tartaglia, R.I. Morimoto, C.M. Dobson, M. Vendruscolo,
700 Widespread aggregation and neurodegenerative diseases are associated with
701 supersaturated proteins, Cell Rep 5(3) (2013) 781-90.
702 [26] P. Ciryam, R. Kundra, R.I. Morimoto, C.M. Dobson, M. Vendruscolo,
703 Supersaturation is a major driving force for protein aggregation in
704 neurodegenerative diseases, Trends Pharmacol Sci 36(2) (2015) 72-7.
705 [27] S. Boeynaems, E. Bogaert, D. Kovacs, A. Konijnenberg, E. Timmerman, A.
706 Volkov, M. Guharoy, M. De Decker, T. Jaspers, V.H. Ryan, A.M. Janke, P. Baatsen, T.
707 Vercruysse, R.M. Kolaitis, D. Daelemans, J.P. Taylor, N. Kedersha, P. Anderson, F.
708 Impens, F. Sobott, J. Schymkowitz, F. Rousseau, N.L. Fawzi, W. Robberecht, P. Van
709 Damme, P. Tompa, L. Van Den Bosch, Phase Separation of C9orf72 Dipeptide
710 Repeats Perturbs Stress Granule Dynamics, Mol Cell 65(6) (2017) 1044-1055 e5.
711 [28] A. Hershko, A. Ciechanover, The ubiquitin system, Annu Rev Biochem 67
712 (1998) 425-79.
713 [29] A. Ciechanover, P. Brundin, The ubiquitin proteasome system in
714 neurodegenerative diseases: sometimes the chicken, sometimes the egg, Neuron
715 40(2) (2003) 427-46.
716 [30] C.M. Pickart, Mechanisms underlying ubiquitination, Annu Rev Biochem 70
717 (2001) 503-33.
718 [31] N.P. Dantuma, T.A. Groothuis, F.A. Salomons, J. Neefjes, A dynamic ubiquitin
719 equilibrium couples proteasomal activity to chromatin remodeling, J Cell Biol
720 173(1) (2006) 19-26.
721 [32] T.A. Groothuis, N.P. Dantuma, J. Neefjes, F.A. Salomons, Ubiquitin crosstalk
722 connecting cellular processes, Cell Div 1 (2006) 21.
723 [33] B.J. Turner, J.D. Atkin, M.A. Farg, D.W. Zang, A. Rembach, E.C. Lopes, J.D.
724 Patch, A.F. Hill, S.S. Cheema, Impaired extracellular secretion of mutant
725 superoxide dismutase 1 associates with neurotoxicity in familial amyotrophic
726 lateral sclerosis, J Neurosci 25(1) (2005) 108-17.
727 [34] S. Bergink, F.A. Salomons, D. Hoogstraten, T.A. Groothuis, H. de Waard, J. Wu,
728 L. Yuan, E. Citterio, A.B. Houtsmuller, J. Neefjes, J.H. Hoeijmakers, W. Vermeulen,
729 N.P. Dantuma, DNA damage triggers nucleotide excision repair-dependent
730 monoubiquitylation of histone H2A, Genes Dev 20(10) (2006) 1343-52.
731 [35] N.R. Cashman, H.D. Durham, J.K. Blusztajn, K. Oda, T. Tabira, I.T. Shaw, S.
732 Dahrouge, J.P. Antel, Neuroblastoma x spinal cord (NSC) hybrid cell lines
733 resemble developing motor neurons, Dev Dyn 194(3) (1992) 209-21.
734 [36] S. Yang, K.Y. Zhang, R. Kariawasam, M. Bax, J.A. Fifita, L. Ooi, J.J. Yerbury, G.A.
735 Nicholson, I.P. Blair, Evaluation of Skin Fibroblasts from Amyotrophic Lateral
736 Sclerosis Patients for the Rapid Study of Pathological Features, Neurotox Res
737 28(2) (2015) 138-46.

[37] C.A. Schneider, W.S. Rasband, K.W. Eliceiri, NIH Image to ImageJ: 25 years of image analysis, Nat Methods 9(7) (2012) 671-5.
[38] S.R. Nagarajan, A.E. Brandon, J.A. McKenna, H.C. Shtein, T.Q. Nguyen, E. Suryana, P. Poronnik, G.J. Cooney, D.N. Saunders, A.J. Hoy, Insulin and diet-induced changes in the ubiquitin-modified proteome of rat liver, PLoS One 12(3) (2017) e0174431.
[39] B. Turriziani, A. Garcia-Munoz, R. Pilkington, C. Raso, W. Kolch, A. von Kriegsheim, On-beads digestion in conjunction with data-dependent mass spectrometry: a shortcut to quantitative and dynamic interaction proteomics, Biology (Basel) 3(2) (2014) 320-32.
[40] J. Cox, M. Mann, MaxQuant enables high peptide identification rates, individualized p.p.b.-range mass accuracies and proteome-wide protein quantification, Nat Biotechnol 26(12) (2008) 1367-72.
[41] D.R. Croucher, M. Iconomou, J.F. Hastings, S.P. Kennedy, J.Z. Han, R.F. Shearer, J. McKenna, A. Wan, J. Lau, S. Aparicio, D.N. Saunders, Bimolecular complementation affinity purification (BiCAP) reveals dimer-specific protein interactions for ERBB2 dimers, Sci Signal 9(436) (2016) ra69.
[42] D. Szklarczyk, A. Franceschini, S. Wyder, K. Forslund, D. Heller, J. Huerta-Cepas, M. Simonovic, A. Roth, A. Santos, K.P. Tsafou, M. Kuhn, P. Bork, L.J. Jensen, C. von Mering, STRING v10: protein-protein interaction networks, integrated over the tree of life, Nucleic Acids Res 43(Database issue) (2015) D447-52.
[43] M.E. Smoot, K. Ono, J. Ruscheinski, P.L. Wang, T. Ideker, Cytoscape 2.8: new features for data integration and network visualization, Bioinformatics 27(3) (2011) 431-2.
[44] R.K. Dagda, S.J. Cherra, 3rd, S.M. Kulich, A. Tandon, D. Park, C.T. Chu, Loss of PINK1 function promotes mitophagy through effects on oxidative stress and mitochondrial fission, J Biol Chem 284(20) (2009) 13843-55.
[45] N.E. Farrawell, I.A. Lambert-Smith, S.T. Warraich, I.P. Blair, D.N. Saunders, D.M. Hatters, J.J. Yerbury, Distinct partitioning of ALS associated TDP-43, FUS and SOD1 mutants into cellular inclusions, Sci Rep 5 (2015) 13416.
[46] N.F. Bence, R.M. Sampat, R.R. Kopito, Impairment of the ubiquitin-proteasome system by protein aggregation, Science 292(5521) (2001) 1552-5.
[47] M. Mattiazzi, M. D'Aurelio, C.D. Gajewski, K. Martushova, M. Kiaei, M.F. Beal, G. Manfredi, Mutated human SOD1 causes dysfunction of oxidative phosphorylation in mitochondria of transgenic mice, J Biol Chem 277(33) (2002) 29626-33.
[48] C. Vande Velde, K.K. McDonald, Y. Boukhedimi, M. McAlonis-Downes, C.S. Lobsiger, S. Bel Hadj, A. Zandona, J.P. Julien, S.B. Shah, D.W. Cleveland, Misfolded SOD1 associated with motor neuron mitochondria alters mitochondrial shape and distribution prior to clinical onset, PLoS One 6(7) (2011) e22031.
[49] W. Song, Y. Song, B. Kincaid, B. Bossy, E. Bossy-Wetzel, Mutant SOD1G93A triggers mitochondrial fragmentation in spinal cord motor neurons: neuroprotection by SIRT3 and PGC-1alpha, Neurobiol Dis 51 (2013) 72-81.
[50] J. Lowe, A. Blanchard, K. Morrell, G. Lennox, L. Reynolds, M. Billett, M. Landon, R.J. Mayer, Ubiquitin is a common factor in intermediate filament inclusion bodies of diverse type in man, including those of Parkinson's disease, Pick's disease, and Alzheimer's disease, as well as Rosenthal fibres in cerebellar astrocytomas, cytoplasmic bodies in muscle, and mallory bodies in alcoholic liver disease, J Pathol 155(1) (1988) 9-15.

787 [51] H. Mori, J. Kondo, Y. Ihara, Ubiquitin is a component of paired helical
788 filaments in Alzheimer's disease, Science 235(4796) (1987) 1641-4.
789 [52] E.L. Scotter, C. Vance, A.L. Nishimura, Y.B. Lee, H.J. Chen, H. Urwin, V.
790 Sardone, J.C. Mitchell, B. Rogelj, D.C. Rubinsztein, C.E. Shaw, Differential roles of
791 the ubiquitin proteasome system and autophagy in the clearance of soluble and
792 aggregated TDP-43 species, J Cell Sci 127(Pt 6) (2014) 1263-78.
793 [53] K. Miyazaki, T. Fujita, T. Ozaki, C. Kato, Y. Kurose, M. Sakamoto, S. Kato, T.
794 Goto, Y. Itoyama, M. Aoki, A. Nakagawara, NEDL1, a novel ubiquitin-protein
795 isopeptide ligase for dishevelled-1, targets mutant superoxide dismutase-1, J Biol
796 Chem 279(12) (2004) 11327-35.
797 [54] J.M. Tan, E.S. Wong, D.S. Kirkpatrick, O. Pletnikova, H.S. Ko, S.P. Tay, M.W. Ho,
798 J. Troncoso, S.P. Gygi, M.K. Lee, V.L. Dawson, T.M. Dawson, K.L. Lim, Lysine 63-
799 linked ubiquitination promotes the formation and autophagic clearance of
800 protein inclusions associated with neurodegenerative diseases, Hum Mol Genet
801 17(3) (2008) 431-9.
802 [55] H. Wang, Z. Ying, G. Wang, Ataxin-3 regulates aggresome formation of
803 copper-zinc superoxide dismutase (SOD1) by editing K63-linked polyubiquitin
804 chains, J Biol Chem 287(34) (2012) 28576-85.
805 [56] A.M. Mabb, M.D. Ehlers, Ubiquitination in postsynaptic function and
806 plasticity, Annu Rev Cell Dev Biol 26 (2010) 179-210.
807 [57] H. Kawabe, N. Brose, The role of ubiquitylation in nerve cell development,
808 Nat Rev Neurosci 12(5) (2011) 251-68.
809 [58] Y. Tashiro, M. Urushitani, H. Inoue, M. Koike, Y. Uchiyama, M. Komatsu, K.
810 Tanaka, M. Yamazaki, M. Abe, H. Misawa, K. Sakimura, H. Ito, R. Takahashi, Motor
811 neuron-specific disruption of proteasomes, but not autophagy, replicates
812 amyotrophic lateral sclerosis, J Biol Chem 287(51) (2012) 42984-94.
813 [59] C. Cheroni, M. Marino, M. Tortarolo, P. Veglianese, S. De Biasi, E. Fontana,
814 L.V. Zuccarello, C.J. Maynard, N.P. Dantuma, C. Bendotti, Functional alterations of
815 the ubiquitin-proteasome system in motor neurons of a mouse model of familial
816 amyotrophic lateral sclerosis, Hum Mol Genet 18(1) (2009) 82-96.
817 [60] P. Ciryam, R. Kundra, R. Freer, R.I. Morimoto, C.M. Dobson, M. Vendruscolo,
818 A transcriptional signature of Alzheimer's disease is associated with a
819 metastable subproteome at risk for aggregation, Proc Natl Acad Sci U S A
820 113(17) (2016) 4753-8.
821 [61] Z. Tan, W. Qu, W. Tu, W. Liu, M. Baudry, S.S. Schreiber, p53 accumulation due
822 to down-regulation of ubiquitin: relevance for neuronal apoptosis, Cell Death
823 Differ 7(7) (2000) 675-81.
824 [62] Z. Tan, W. Tu, S.S. Schreiber, Downregulation of free ubiquitin: a novel
825 mechanism of p53 stabilization and neuronal cell death, Brain Res Mol Brain Res
826 91(1-2) (2001) 179-88.
827 [63] E.G. Mimnaugh, H.Y. Chen, J.R. Davie, J.E. Celis, L. Neckers, Rapid
828 deubiquitination of nucleosomal histones in human tumor cells caused by
829 proteasome inhibitors and stress response inducers: effects on replication,
830 transcription, translation, and the cellular stress response, Biochemistry 36(47)
831 (1997) 14418-29.
832 [64] A. Patnaik, V. Chau, J.W. Wills, Ubiquitin is part of the retrovirus budding
833 machinery, Proc Natl Acad Sci U S A 97(24) (2000) 13069-74.
834 [65] J. Hanna, D.S. Leggett, D. Finley, Ubiquitin depletion as a key mediator of
835 toxicity by translational inhibitors, Mol Cell Biol 23(24) (2003) 9251-61.

[66] J.H. Vaden, J.A. Watson, A.D. Howard, P.C. Chen, J.A. Wilson, S.M. Wilson, Distinct effects of ubiquitin overexpression on NMJ structure and motor performance in mice expressing catalytically inactive USP14, Front Mol Neurosci 8 (2015) 11.
[67] A. Hyrskyluoto, C. Bruelle, S.H. Lundh, H.T. Do, J. Kivinen, E. Rappou, S. Reijonen, T. Waltimo, A. Petersen, D. Lindholm, L. Korhonen, Ubiquitin-specific protease-14 reduces cellular aggregates and protects against mutant huntingtin-induced cell degeneration: involvement of the proteasome and ER stress-activated kinase IRE1alpha, Hum Mol Genet (2014).
[68] E. Kiskinis, J. Sandoe, L.A. Williams, G.L. Boulting, R. Moccia, B.J. Wainger, S. Han, T. Peng, S. Thams, S. Mikkilineni, C. Mellin, F.T. Merkle, B.N. Davis-Dusenbery, M. Ziller, D. Oakley, J. Ichida, S. Di Costanzo, N. Atwater, M.L. Maeder, M.J. Goodwin, J. Nemesh, R.E. Handsaker, D. Paull, S. Noggle, S.A. McCarroll, J.K. Joung, C.J. Woolf, R.H. Brown, K. Eggan, Pathways disrupted in human ALS motor neurons identified through genetic correction of mutant SOD1, Cell Stem Cell 14(6) (2014) 781-95.
[69] S. Maharjan, M. Oku, M. Tsuda, J. Hoseki, Y. Sakai, Mitochondrial impairment triggers cytosolic oxidative stress and cell death following proteasome inhibition, Sci Rep 4 (2014) 5896.
[70] A. Ugun-Klusek, M.H. Tatham, J. Elkharaz, D. Constantin-Teodosiu, K. Lawler, H. Mohamed, S.M. Paine, G. Anderson, R. John Mayer, J. Lowe, E. Ellen Billett, L. Bedford, Continued 26S proteasome dysfunction in mouse brain cortical neurons impairs autophagy and the Keap1-Nrf2 oxidative defence pathway, Cell Death Dis 8(1) (2017) e2531.
[71] C. Vijayvergiya, M.F. Beal, J. Buck, G. Manfredi, Mutant superoxide dismutase 1 forms aggregates in the brain mitochondrial matrix of amyotrophic lateral sclerosis mice, J Neurosci 25(10) (2005) 2463-70.
[72] D. Jaarsma, F. Rognoni, W. van Duijn, H.W. Verspaget, E.D. Haasdijk, J.C. Holstege, CuZn superoxide dismutase (SOD1) accumulates in vacuolated mitochondria in transgenic mice expressing amyotrophic lateral sclerosis-linked SOD1 mutations, Acta Neuropathol 102(4) (2001) 293-305.
[73] L. Ruan, C. Zhou, E. Jin, A. Kucharavy, Y. Zhang, Z. Wen, L. Florens, R. Li, Cytosolic proteostasis through importing of misfolded proteins into mitochondria, Nature (2017).
[74] R. Yonashiro, A. Sugiura, M. Miyachi, T. Fukuda, N. Matsushita, R. Inatome, Y. Ogata, T. Suzuki, N. Dohmae, S. Yanagi, Mitochondrial ubiquitin ligase MITOL ubiquitinates mutant SOD1 and attenuates mutant SOD1-induced reactive oxygen species generation, Mol Biol Cell 20(21) (2009) 4524-30.

Declarations

Ethics approval and consent to participate
Not applicable

Consent for publication
Not applicable

Availability of data and material
The datasets used and/or analysed during the current study available from the corresponding author on reasonable request.

Competing interests
The authors declare that they have no competing interests

Funding
I.A.L.S was supported by Rotary Health Australia. P.C. was supported by grants from the US-UK Fulbright Commission, St. John's College, University of Cambridge, and the National Institutes of Health (Northwestern University Medical Scientist Training Program Grant T32 GM8152-28). D.N.S, K.L.V and J.J.Y were supported by US Department of Defence (AL150057) and the Motor Neuron Disease Research Institute of Australia (Cunningham Family MND Research Grant, GIA1656).
J.J.Y was also supported by grants from the National Health and Medical Research Council (1095215, 1084144).

Authors' contributions
N.E.F, P.C, L.M, K.L.V, D.N.S, and J.J.Y designed research; N.E.F, P.C, I.A.L.S, L.M, J.M, and K.M performed research; N.E.F, I.A.L.S, P.C, L.M, K.L.V, D.N.S, and J.J.Y analyzed data; and N.E.F, P.C, D.N.S, and J.J.Y wrote the paper. All authors read and approved the final manuscript.

Acknowledgements
Not applicable

Authors' information (optional)

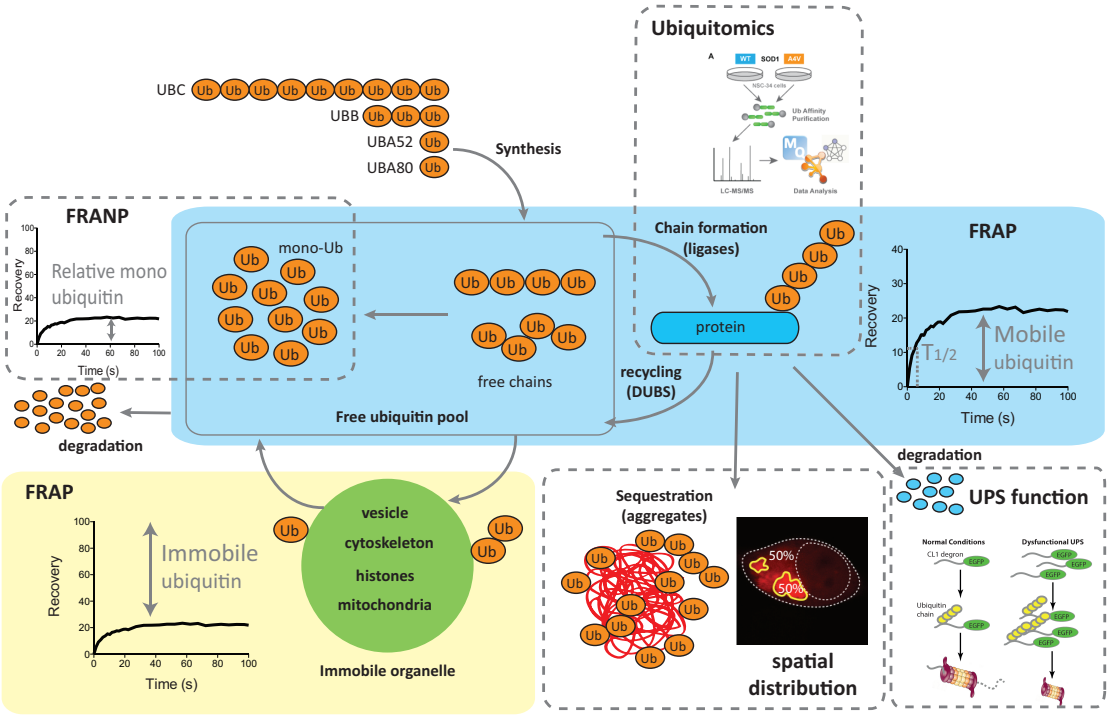

Figure 1: Ubiquitin exists in a dynamic equilibrium in the cell, partitioning into mobile and immobile fractions. Schematic representation of Ub homeostasis, showing the different methods used to interrogate various aspects of this system in this study. Ub is synthesised from several genes, generating a pool of free Ub that consists of monomeric and polymeric chains of Ub. Ub can be conjugated with substrate proteins via the enzymatic activity of a large number of Ub ligases. The cellular fate or outcome of such ubiquitylation is dictated by the chain type formed by Ub. The mobile fraction of Ub measured by fluorescence recovery after photobleaching (FRAP) is the sum of monomeric and polymeric free Ub and diffusible ubiquitylated protein (blue box). The immobile pool of Ub is that conjugated to large slowly diffusing structures such as vesicles, organelles, histones and cytoskeleton (green box). Ubiquitin proteasome system (UPS) degradation function can be compared using fluorescent reporters. Generally accumulation of reporters suggests increased competition, or decreased rates of degradation. The ubiquitin-modified proteome can be quantified using enrichment capture and mass spectrometry (ubiqitomics). A subset of mobile Ub is free monomeric Ub can be measured using fluorescence recovery after nucleus photobleaching (FRANP). Monomeric Ub is the only form of tagged Ub that can diffuse through the nuclear pore, so by bleaching the entire nucleus we can measure monomeric Ub as it diffuses back in. In the context of protein aggregation a proportion of Ub is conjugated to substrates within the inclusions, we can quantify the proportion of Ub incorporated into inclusions using image analysis.

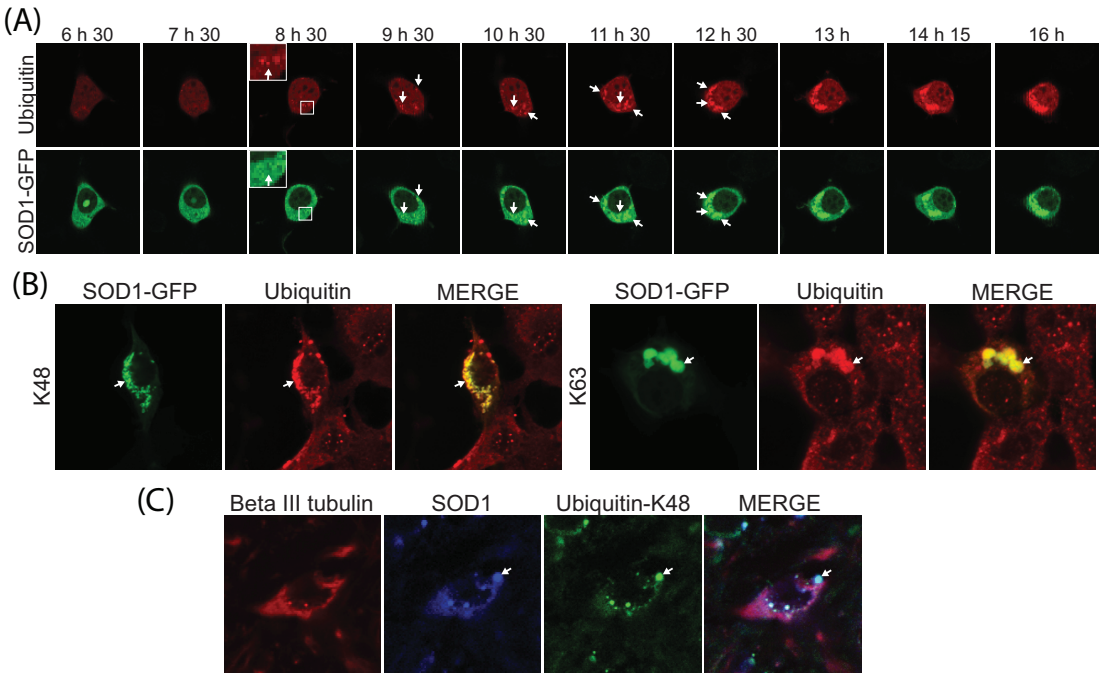

Figure 2: SOD1 co-aggregates with ubiquitin. (A) NSC-34 cells co-transfected with $SOD1^{A4V}$-GFP and mRFP-Ub were imaged every 15 min for 17 h. (B) NSC-34 cells overexpressing $SOD1^{A4V}$-GFP were fixed, permeabilized and stained for Ub_{K48} and Ub_{K63} polyubiquitin chains 48 h post transfection. (C) Spinal cord from the $SOD1^{G93A}$ mouse was fixed, permeabilized and stained for neuron-specific beta III tubulin, SOD1 and Ub_{K48}. Co-localization of SOD1 and Ub is indicated with arrows.

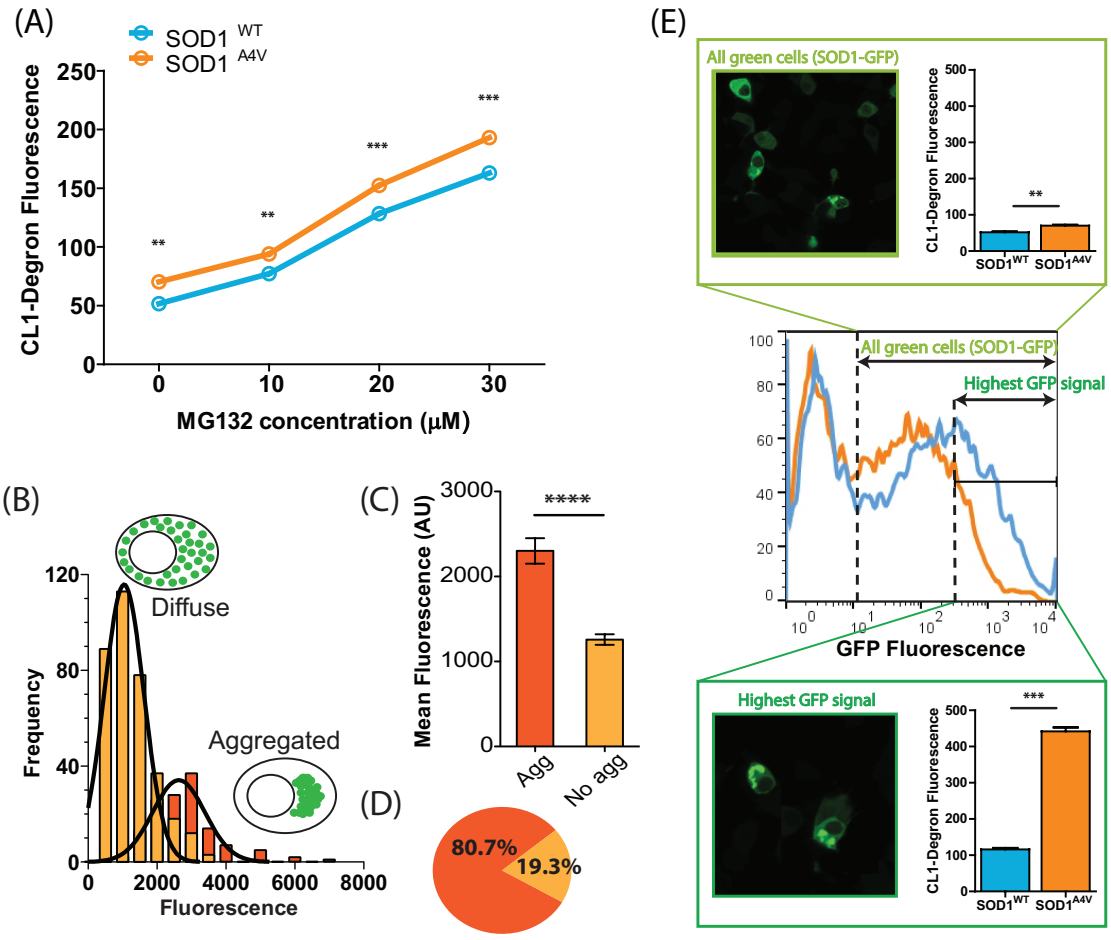

Figure 3: Mutant SOD1^{A4V} alters UPS activity. (A) Dose dependant response of UPS activity (tdTomato^{CL1} fluorescence) in NSC-34 cells co-transfected with SOD1-GFP after overnight treatment with the proteasome inhibitor MG132. Data represent mean CL1-Degron fluorescence ± SEM (n=3), ** P< 0.01; *** P<0.001. (B) Frequency distribution analysis of SOD1-GFP fluorescence was performed on cells expressing soluble (diffuse) SOD1^{A4V} and aggregated SOD1^{A4V}. (C) Cells containing SOD1^{A4V} aggregates exhibited significantly higher fluorescence than cells that did not contain aggregates, **** P< 0.0001. (D) 80% of cells expressing the highest SOD1-GFP signal (top 10%) contained aggregates. (E) Cells expressing the highest GFP signal typically contained aggregates and revealed greater significant differences in tdTomato^{CL1} fluorescence between cells expressing SOD1^{WT} and SOD1^{A4V}.

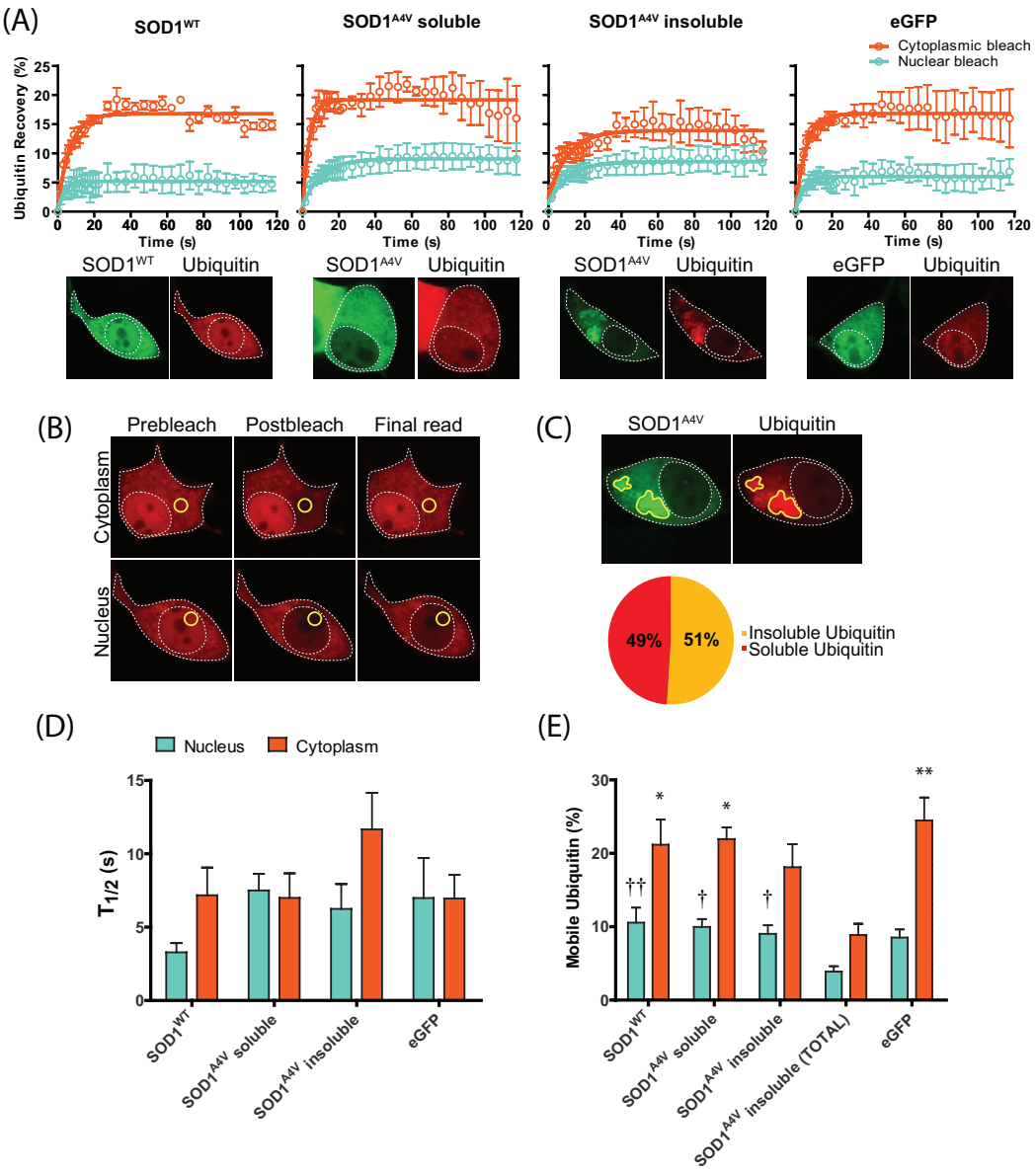

Figure 4: Ubiquitin distribution is altered in cells containing SOD1^{A4V} aggregates. (A) NSC-34 cells co-transfected with SOD1-GFP and mCherry-Ub were photobleached in either the nucleus or cytoplasm and recovery of Ub fluorescence was monitored for 120 s. Data shown are means ± SEM (n=3) and are representative of 3 independent experiments. (B) Representative confocal images of pre-bleach, post-bleach and recovery endpoint are shown with the ROI marked in yellow. (C) The amount of Ub incorporated into SOD1^{A4V} inclusions was quantified using ImageJ. (D) Diffusion rates of mCherry-Ub measured in both the nucleus and cytoplasm of co-transfected NSC-34 cells. Error bars are SEM ($n \geq 6$, combined from 3 independent experiments). (E) Quantification of the proportion of mobile Ub in the nucleus and cytoplasm of cells expressing either SOD1^{WT}, soluble SOD1^{A4V} or insoluble SOD1^{A4V}. SOD1^{A4V} insoluble (TOTAL) represents total Ub levels taking into account the proportion of Ub incorporated into SOD1 inclusions (determined in (C)). Data shown are means ± SEM combined from 3 independent experiments ($n \geq 7$). One way Anova was used to compare differences. * and † indicate significant difference to SOD1^{A4V} insoluble (TOTAL) in the cytoplasm and nucleus respectively. * † $P < 0.05$, ** † † $P < 0.01$.

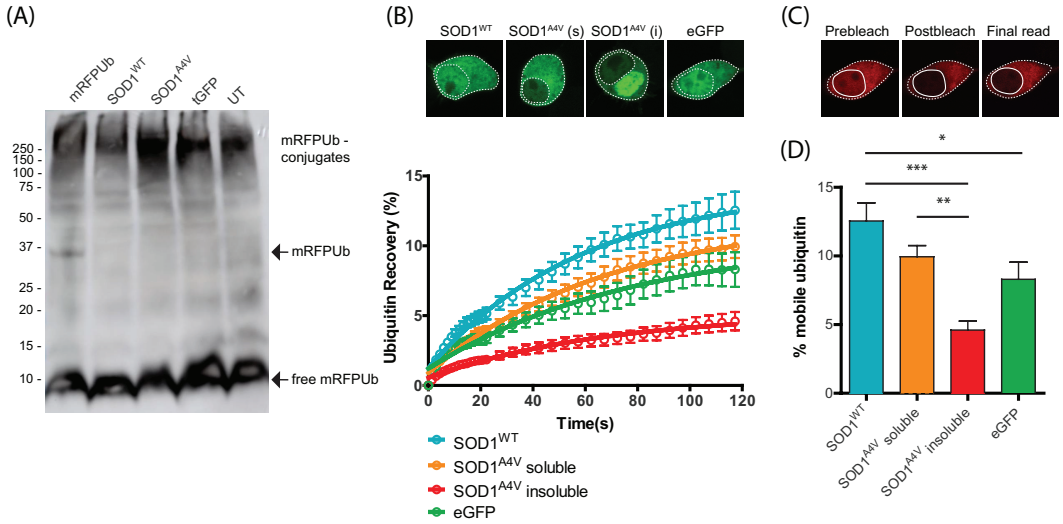

Figure 5: Reduced levels of free monomeric ubiquitin in NSC-34 cells containing SOD1^{A4V} aggregates. (A) Western blot analysis of cell lysates of NSC-34 cells transiently transfected with SOD1-GFP, mRFP-Ub or eGFP control. Samples were separated under reducing conditions and probed with anti-ubiquitin antibody. (B) The entire nucleus of co-transfected NSC-34 cells was photobleached and the recovery of nuclear Ub was monitored as a proportion of cytoplasmic fluorescence for 120 s. Data shown are means ± SEM ($n \geq 17$) combined from 3 independent experiments. (C) Representative confocal images of pre-bleach, post-bleach and final read. (D). The percentage of mobile Ub in the nucleus at the final read was quantified as a proportion of cytoplasmic fluorescence. Data represent mean ± SEM ($n \geq 17$, combined from 3 independent experiments)* $P < 0.05$, ** $P < 0.01$, *** $P<0.001$.

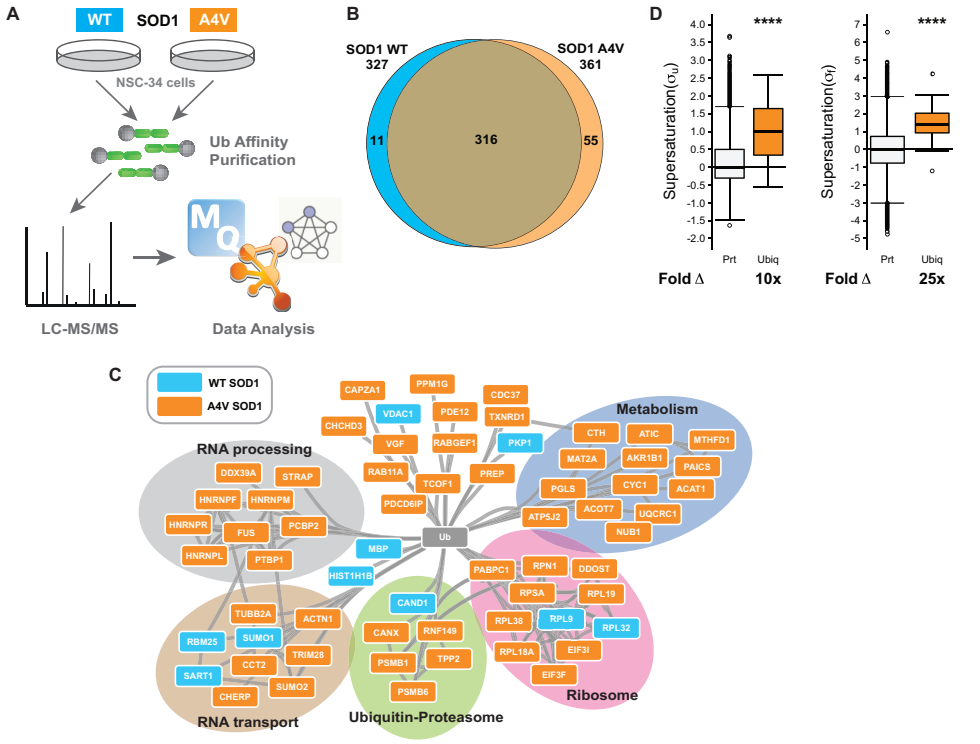

Figure 6: The ubiquitylated proteome of transfected NSC-34 cells. (A) NSC-34 cells expressing GFP fusions of $SOD1^{WT}$ or $SOD1^{A4V}$ were subjected to high affinity purification to isolate ubiquitylated proteins which were subsequently identified by LC-MS/MS. (B) Venn analysis comparing the number of ubiquitylated proteins in NSC-34 cells transfected with either $SOD1^{A4V}$ (n=2) or $SOD1^{WT}$ (n=3). (C) STRING analysis of protein-protein interaction network of ubiquitylated proteins unique to either $SOD1^{A4V}$ or $SOD1^{WT}$. Proteins were identified as present in each condition if they were present in at least two replicates for that condition. Additionally proteins were only considered "unique" to either $SOD1^{WT}$ or $SOD1^{A4V}$ if they were not identified in any of the replicates for any of the other conditions. (D) The median supersaturation score calculated for the unfolded ($\boldsymbol{\sigma}_u$) and native ($\boldsymbol{\sigma}_f$) states of proteins unique to the $SOD1^{A4V}$ ubiquitome. Fold **Δ** refers to the increase in supersaturation score from the known mouse proteome.

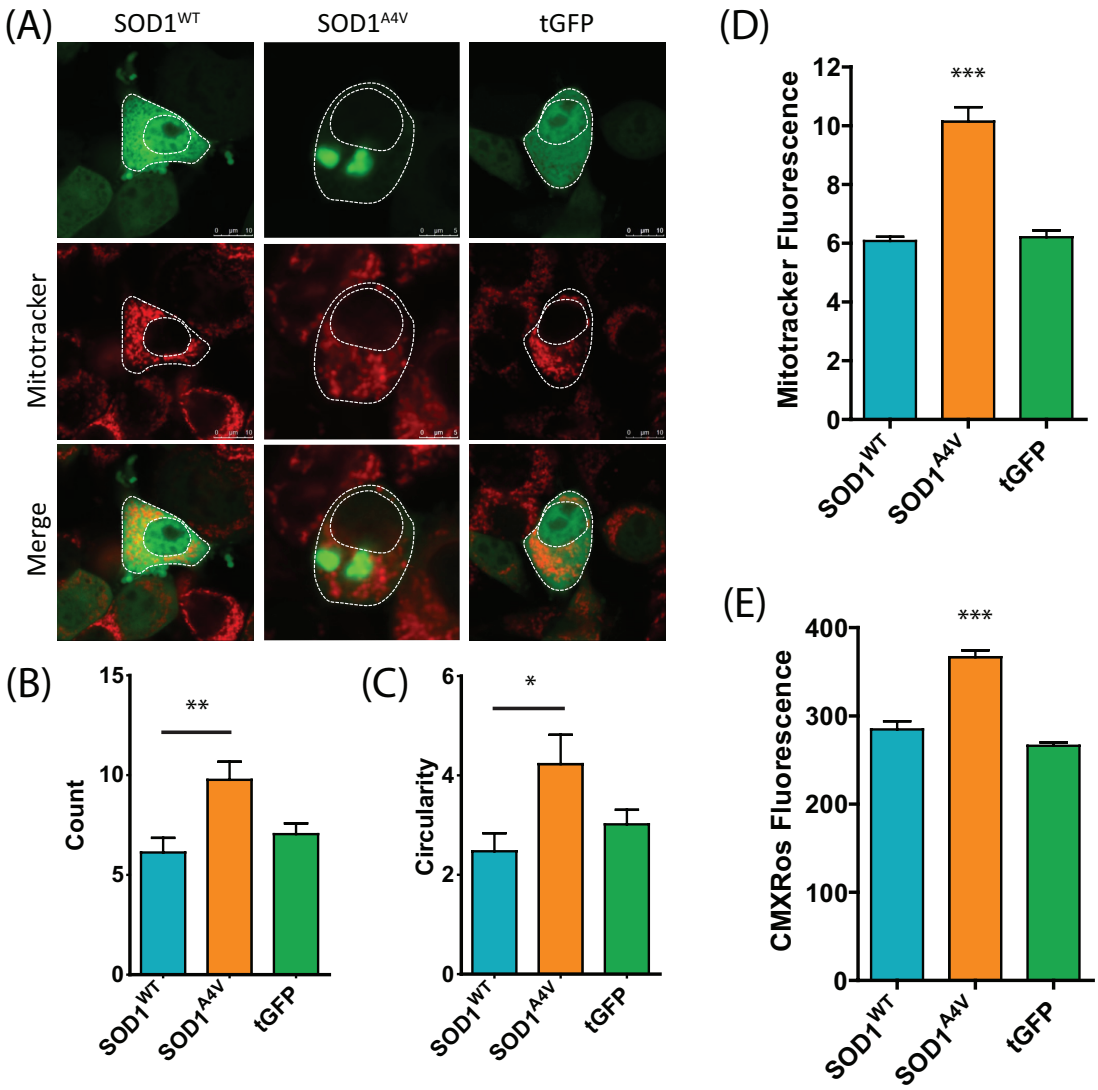

Figure 7: Cells containing SOD1 aggregates display altered mitochondrial morphology and dysfunction. (A) NSC-34 cells transiently transfected with SOD1-GFP were stained for mitochondria 48 h post transfection with Mitotracker Deep Red. The number of mitochondria (B) and circularity (C) was determined using a mitochondrial morphology macro in ImageJ. Data represent mean ± SEM ($n \geq 23$) * $P < 0.05$, ** $P < 0.01$. (D) Mitotracker fluorescence was also quantified by flow cytometry in cells expressing the highest levels of SOD1-GFP. (E) Mitochondrial membrane potential was examined through the accumulation of Mitotracker Red CMXRos. Data represent mean ± SEM ($n = 3$) *** $P<0.001$.

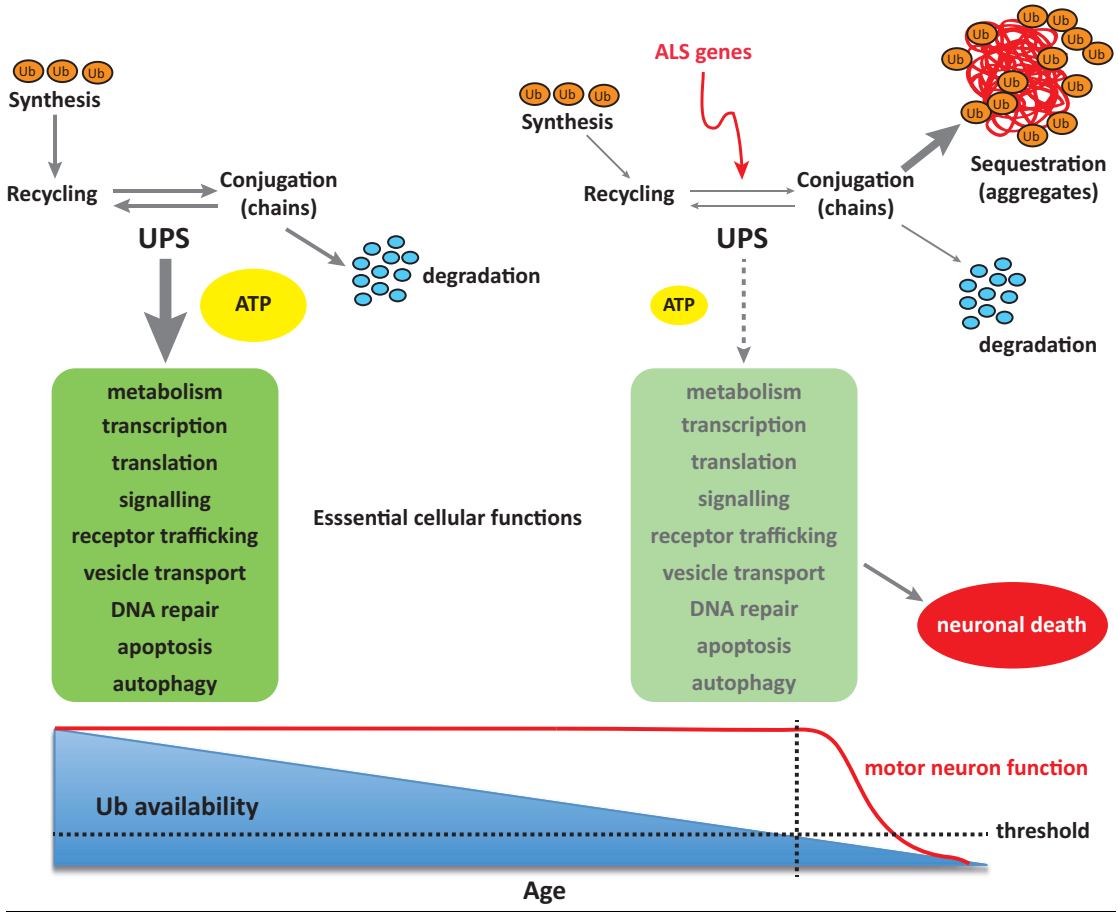

Figure 8: Disrupted Ub homeostasis in ALS. Mutations in SOD1-associated ALS disrupt Ub homeostasis, either directly or through sequestration of Ub into protein aggregates. These changes result in altered Ub distribution and subsequent depletion of free Ub, eventually reaching a threshold below which vital cellular functions are severely compromised, and ultimately result in cell death.

Table 1. Proteins identified unique to A4V or WT SOD1:

Unique to SOD^{1A4V}

Entry	Entry name	Protein names	Gene names	Unique peptides
P14206	RSSA_MOUSE	40S ribosomal protein SA	Rpsa Lamr1 P40-8	5
P47753	CAZA1_MOUSE	F-actin-capping protein subunit alpha-1	Capza1 Cappa1	3
Q91V12	BACH_MOUSE	Cytosolic acyl coenzyme A thioester hydrolase	Acot7 Bach	3
Q9QUR6	PPCE_MOUSE	Prolyl endopeptidase	Prep Pep	4
Q922D8	C1TC_MOUSE	C-1-tetrahydrofolate synthase	Mthfd1	2
P45376	ALDR_MOUSE	Aldose reductase	Akr1b1 Akr1b3 Aldor1 Aldr1	4
Q8CGZ0	CHERP_MOUSE	Calcium homeostasis endoplasmic reticulum protein	Cherp Scaf6	3
Q8R081	HNRPL_MOUSE	Heterogeneous nuclear ribonucleoprotein L	Hnrnpl Hnrpl	2
O08784	TCOF_MOUSE	Treacle protein	Tcof1	2
O09061	PSB1_MOUSE	Proteasome subunit beta type-1	Psmb1	2
O54734	OST48_MOUSE	Dolichyl-diphosphooligosaccharide--protein glycosyltransferase 48 kDa subunit	Ddost	4
P29341	PABP1_MOUSE	Polyadenylate-binding protein 1	Pabpc1 Pabp1	4
P35564	CALX_MOUSE	Calnexin	Canx	5
P62492	RB11A_MOUSE	Ras-related protein Rab-11A	Rab11a Rab11	2
P54729	NUB1_MOUSE	NEDD8 ultimate buster 1	Nub1 Nyren18	2
P56135	ATPK_MOUSE	ATP synthase subunit f, mitochondrial	Atp5j2	2
P56959	FUS_MOUSE	RNA-binding protein FUS	Fus	3
Q7TPR4	ACTN1_MOUSE	Alpha-actinin-1	Actn1	5
P61957	SUMO2_MOUSE	Small ubiquitin-related modifier 2	Sumo2 Smt3b Smt3h2	2
P62717	RL18A_MOUSE	60S ribosomal protein L18a	Rpl18a	4

Q3THS6	METK2_MOUSE	S-adenosylmethionine synthase isoform type-2 (AdoMet synthase 2)	Mat2a	2
Q3TIU4	PDE12_MOUSE	2',5'-phosphodiesterase 12 (2'-PDE) (2-PDE)	Pde12	2
Q3U2C5	RN149_MOUSE	E3 ubiquitin-protein ligase RNF149	Rnf149 Greul4	2
Q60692	PSB6_MOUSE	Proteasome subunit beta type-6	Psmb6 Lmp19	3
Q61074	PPM1G_MOUSE	Protein phosphatase 1G	Ppm1g Fin13 Ppm1c	3
Q61081	CDC37_MOUSE	Hsp90 co-chaperone Cdc37	Cdc37	2
Q61990	PCBP2_MOUSE	Poly(rC)-binding protein 2 (Alpha-CP2)	Pcbp2 Cbp Hnrnpx Hnrpx	2
Q62318	TIF1B_MOUSE	Transcription intermediary factor 1-beta (TIF1-beta) (E3 SUMO-protein ligase TRIM28)	Trim28 Kap1 Krip1 Tif1b	4
Q64514	TPP2_MOUSE	Tripeptidyl-peptidase 2 (TPP-2)	Tpp2	2
Q8QZT1	THIL_MOUSE	Acetyl-CoA acetyltransferase, mitochondrial	Acat1	2
Q8VCN5	CGL_MOUSE	Cystathionine gamma-lyase	Cth	3
Q8VDW0	DX39A_MOUSE	ATP-dependent RNA helicase DDX39A	Ddx39a Ddx39	2
Q7TMK9	HNRPQ_MOUSE	Heterogeneous nuclear ribonucleoprotein Q (hnRNP Q)	Syncrip Hnrpq Nsap1 Nsap1l	3
Q91YQ5	RPN1_MOUSE	Dolichyl-diphosphooligosaccharide--protein glycosyltransferase subunit 1	Rpn1	5
P17225	PTBP1_MOUSE	Polypyrimidine tract-binding protein 1 (PTB)	Ptbp1 Ptb	4
Q99LX5	MMTA2_MOUSE	Multiple myeloma tumor-associated protein 2 homolog	Mmtag2	2
Q9CQ60	6PGL_MOUSE	6-phosphogluconolactonase (6PGL)	Pgls	5
Q9CRB9	MIC19_MOUSE	MICOS complex subunit Mic19	Chchd3 Mic19	3
Q9CWF2	TBB2B_MOUSE	Tubulin beta-2B chain	Tubb2b	3
Q9CWJ9	PUR9_MOUSE	Bifunctional purine biosynthesis protein PURH	Atic Purh	4
Q9CZ13	QCR1_MOUSE	Cytochrome b-c1 complex subunit 1, mitochondrial (Complex III subunit 1)	Uqcrc1	4
Q9D0E1	HNRPM_MOUSE	Heterogeneous nuclear ribonucleoprotein M	Hnrnpm Hnrpm	3
Q9D0M3	CY1_MOUSE	Cytochrome c1, heme protein, mitochondrial (Complex III subunit 4)	Cyc1	3
Q9DCH4	EIF3F_MOUSE	Eukaryotic translation initiation factor 3 subunit F	Eif3f Eif3s5	4
Q9DCL9	PUR6_MOUSE	Multifunctional protein ADE2	Paics	5
Q9JJI8	RL38_MOUSE	60S ribosomal protein L38	Rpl38	3
Q9JM13	RABX5_MOUSE	Rab5 GDP/GTP exchange factor	Rabgef1 Rabex5	3

Q9JMH6	TRXR1_MOUSE	Thioredoxin reductase 1, cytoplasmic	Txnrd1 Trxr1	2
Q9QZD9	EIF3I_MOUSE	Eukaryotic translation initiation factor 3 subunit I	Eif3i Eif3s2 Trip1	4
Q9WU78	PDC6I_MOUSE	Programmed cell death 6-interacting protein	Pdcd6ip Aip1 Alix	4
Q9Z1Z2	STRAP_MOUSE	Serine-threonine kinase receptor-associated protein	Strap Unrip	2
Q9Z2X1	HNRPF_MOUSE	Heterogeneous nuclear ribonucleoprotein F	Hnrnpf Hnrpf	3
Unique to SOD^{WT}				
B2RY56	RBM25_MOUSE	RNA-binding protein 25	Rbm25	2
P51410	RL9_MOUSE	60S ribosomal protein L9	Rpl9	5
P04370	MBP_MOUSE	Myelin basic protein	Mbp Shi	4
P43276	H15_MOUSE	Histone H1.5	Hist1h1b H1f5	3
P62911	RL32_MOUSE	60S ribosomal protein L32	Rpl32	3
P63166	SUMO1_MOUSE	Small ubiquitin-related modifier 1 (SUMO-1)	Sumo1 Smt3c Smt3h3 Ubl1	2
P97350	PKP1_MOUSE	Plakophilin-1	Pkp1	17
Q60932	VDAC1_MOUSE	Voltage-dependent anion-selective channel protein 1 (VDAC-1)	Vdac1 Vdac5	8
Q6ZQ38	CAND1_MOUSE	Cullin-associated NEDD8-dissociated protein 1	Cand1 D10Ertd516e Kiaa0829	2
Q7TSF1	DSG1B_MOUSE	Desmoglein-1-beta	Dsg1b Dsg5	6
Q9Z315	SNUT1_MOUSE	U4/U6.U5 tri-snRNP-associated protein 1	Sart1 Haf	2

SOD1^{A4V} aggregation alters ubiquitin homeostasis in a cell model of ALS

Natalie E. Farrawell[1,2], Isabella Lambert-Smith[1,2], Kristen Mitchell[1,2], Jessie McKenna[3], Luke McAlary[1,2,4], Prajwal Ciryam[5,6,7], Kara L. Vine[1,2], Darren N. Saunders[3], Justin J. Yerbury[1,2*]

[1]Illawarra Health and Medical Research Institute, Wollongong, NSW, Australia
[2]School of Biological Sciences, Centre of Medicine and Molecular Bioscience, University of Wollongong, Northfields Ave, Wollongong, NSW, Australia, 2522
[3]School of Medical Sciences, Faculty of Medicine, UNSW Australia
[4]Department of Physics & Astronomy, University of British Columbia, Vancouver, British Columbia, Canada.
[5]Department of Chemistry, University of Cambridge, Cambridge CB2 1EW, UK
[6]Department of Molecular Biosciences, Rice Institute for Biomedical Research, Northwestern University, Evanston, IL 60208-3500, USA
[7]Department of Neurology, Columbia University College of Physicians & Surgeons, New York, NY 10032-3784

Supplementary Methods

To quantify SOD1 inclusion formation, images were acquired as described previously [1]. Briefly, z-stack images of NSC-34 cells transfected with SOD1-GFP constructs were acquired 48 h post transfection using the 63X objective, 512 x 512 pixels, 1 line and frame average and a scan speed of 400 Hz. Z-stacks were processed into a single image using LAS-AF Lite software (Leica) and at least 100 transfected cells were analysed for the presence of inclusions.

Toxicity Assay. The toxicity of cells expressing SOD1 was monitored over 68 h in an Incucyte automated fluorescent microscope (Essen BioScience, USA) as described in [1]. Cells were dissociated 24 h post transfection and replated in 96-well plates at a confluency of 20% in phenol red free DMEM/F12 containing 10% FBS. Images were acquired every 2 h and analysed using a processing definition trained to select GFP positive cells. The number of GFP positive cells was normalised to time zero before SOD1^{A4V} numbers were adjusted to SOD1^{WT} values.

Supplementary Figures

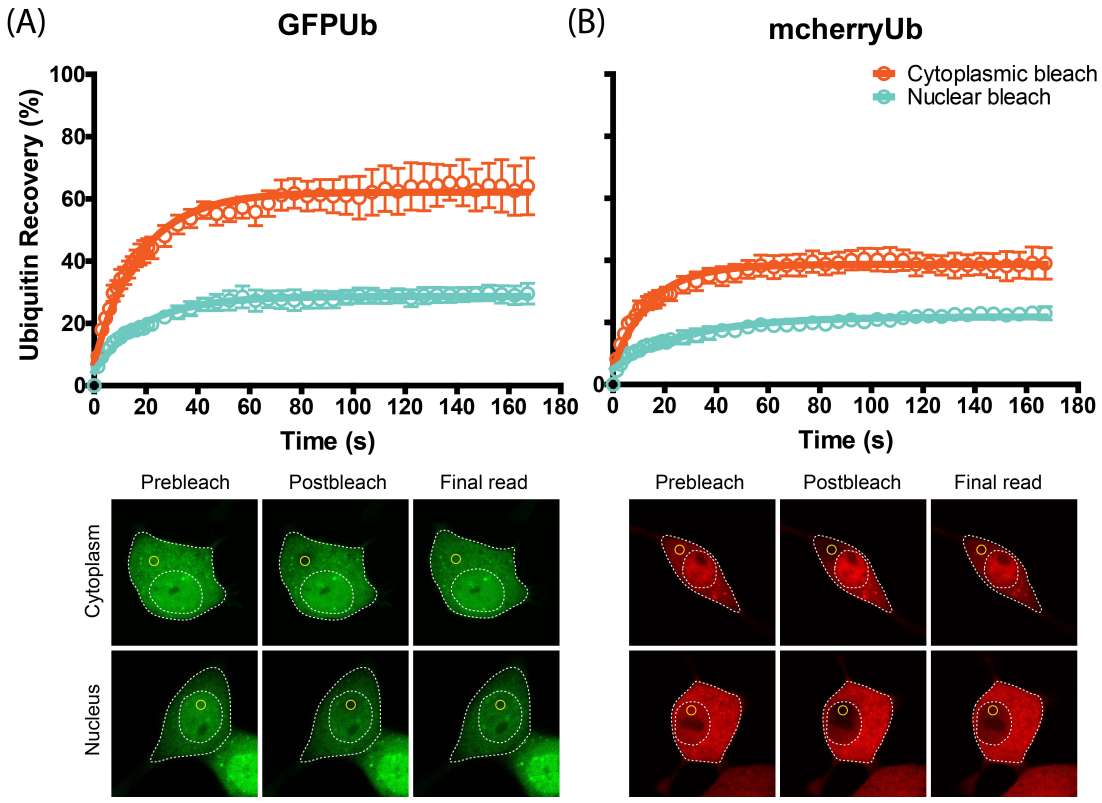

Figure S1: mcherry-Ub behaves in a similar manner to GFP-Ub. (A) NSC-34 cells transfected with either GFP-Ub (A) or mcherry-Ub (B) were photobleached in the cytoplasm or nucleus and recovery of Ub fluorescence was monitored for up to 170 s. Representative confocal images of prebleach, postbleach and recovery endpoint are shown with the ROI marked in yellow.

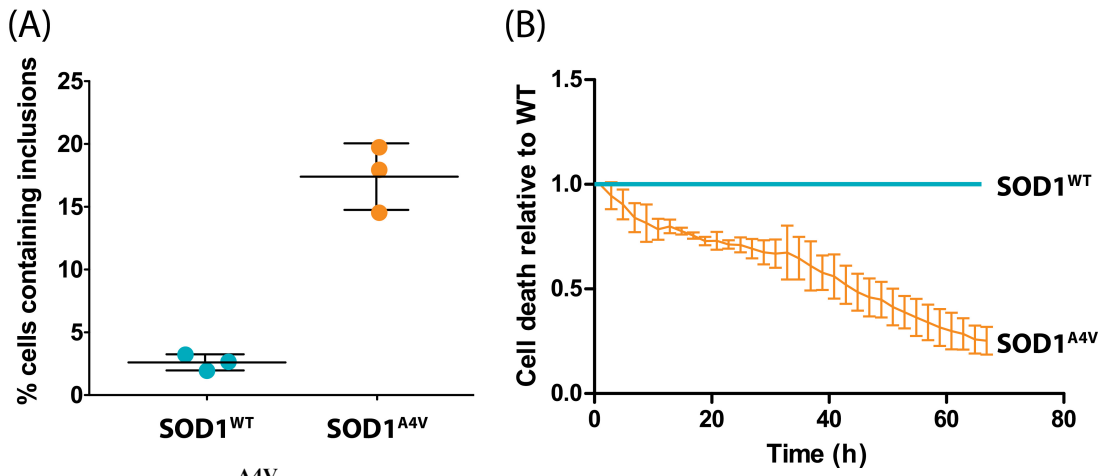

Figure S2: SOD1^{A4V} expression induces inclusion formation and is associated with increased cell death in NSC-34 cells. (A) Inclusion formation in NSC-34 cells expressing SOD1-GFP was determined 48 h post transfection. (B) The toxicity of SOD1^{A4V} was monitored in comparison to SOD1^{WT} over a 68 h period.

[1] L. McAlary, J.A. Aquilina, J.J. Yerbury, Susceptibility of Mutant SOD1 to Form a Destabilized Monomer Predicts Cellular Aggregation and Toxicity but Not In vitro Aggregation Propensity, Front Neurosci 10 (2016) 499.